Volume interdiffusion coefficient and uncertainty assessment for polycrystalline materials

Léchelle, J.[a,*], Noyau S.[a], Aufore L.[a], Arredondo A.[a], Audubert F.[a]

[a]*CEA/DEN DEC/SPUA, Cadarache, bat. 717 - 13115 Saint-Paul-Lez-Durance*

Abstract

A method has been developed in order to assess small volume interdiffusion coefficients from experimental Electron Probe MicroAnalysis concentration profiles of polycrystalline materials by means of Boltzmann-Matano or den Broeder methods and their complementary Hall method. These methods have been used as tools for the investigation of the quasi-binary $UO_2/U_{(1-y)}Pu_yO_{(2-z)}$ interdiffusion, for which obtaining a solid solution in the bulk of grains is of major interest. In this paper uncertainties on the interdiffusion coefficient as a function of concentration have been computed for each method. Small volume coefficient measurements were enhanced by means of a small angle acquisition profile line with respect to the interdiffusion interface.

Keywords: interdiffusion, volume diffusion, Boltzmann-Matano, Hall, den Broeder, uncertainty

1. Introduction

Experimental volume interdiffusion coefficients have to be assessed from binary interdiffusion experiments carried out on polycrystalline materials, as it is often the case in industrial research and development studies. They cannot be simply obtained by means of Boltzmann-Matano [1] [2] or den Broeder [3] methods completed in the plateau areas by Hall [4] method by

---

*mailto:jacques.lechelle@cea.fr

means of discrete integration and derivation techniques from discrete experimental points due to the scattering effect of grain boundary diffusion. Such a problem has often been solved by means of a manual smoothing of the experimental curve [5], or using Oishi model [6]. In this work the problem was sorted out by fitting the diffusion profile with an appropriate function which can afterwards be handled in order to compute the volume diffusion coefficient $\left(\widetilde{D}\right)$ as a function of concentration.

For the three methods uncertainty both upon $\widetilde{D}$ and its variable either the concentration c or the molecular ratio y of the diffusing species has been assessed by means of an error propagation method. J.F.Cornet [5] had coped with this problem by first computing $\widetilde{D}(c)$ versus c, then reassessing the concentration profile from the interdiffusion coefficient and comparing it with the initial experimental profile.

2. Volume interdiffusion information

2.1. Acquiring concentration profiles

Interdiffusion profiles have been acquired by means of an Electron Probe Micro Analyser (EPMA) equipped with an electron gun and 4 wavelength dispersive spectrometers, which allow for simultaneous measurement of the intensity of characteristic X-rays of 4 elements. Quantification of an unknown composition is based on the measurement of standards. The analysed sample line intensity is measured from a sample and from a standard. This standard is a compound with known composition. The measured intensities are corrected for dead time (detector dependent), background and line overlap. The relative intensity ratio of the analysed sample line intensities from sample and standard is calculated. Finally this relative intensity ratio is corrected for the atomic number (Z), absorption (A) and fluorescence (F) effect to give the concentration of the analysed sample. For interdiffusion studies the measurement mode used in EPMA are 1D-line scans. A linescan across a sample is made by moving the sample stage by small $1\mu m$-increments.

2.2. Fitting concentration profiles - Chosing a function

The raw measurement of an EPMA is the weight percent w_e of an element e (in our example U, Pu and O). In this work these raw measurements w_e along the acquisition axis x are first changed into concentration profiles $c_e(x)$

on the basis of the chemical formula of the material (e.g. $U_{(1-x)}Pu_yO_{2-z}$) and of the lattice cell parameter a . The weight percent profiles of several elements may be needed in order to compute the concentration profile of a single element. If we consider U profile:

$$w_U = \frac{(1-y)\,M_U}{(1-y)\,M_U + y\,M_{Pu} + (2-z)\,M_O} \tag{1}$$

where M_U, M_{Pu} and M_O are U, Pu and O molar atomic weight. However in our example we only used one weight percent profile at a time to compute concentration profiles. For this non stoichiometric material z depends only on the plutonium atomic ratio y on the cationic sublattice, on temperature during the interdiffusion experiment and on oxygen partial pressure p_{O_2} (these latter are supposed constant in the volume of the material): $z = f(y, T_{exp.}, p_{O_2})$. y can be deduced from (1) by solving a third degree equation and by means of thermodynamic models ([7],[8] or [9]) in order to compute $f(y, T, p_{O_2})$. Then c_{Pu} can be estimated from the cell parameter a and the thermal expansion coefficient α. $(U_{1-y}, Pu_y)O_{2-z}$ is a Cubic Face Centered (CFC) solid solution the lattice parameter of which is for the 4th order holohedral lattice cell [10]: $a = [(547.0 + 30.1\,z) + (11.0\,z - 7.4)\,y]$ pm and the thermal expansion coefficient of which is $\alpha_{z,T} = \alpha_{z=0,T}(1 + 3.9\,z)$ [10]. The molar volume V_m reads:

$$V_m = \frac{\mathcal{N}}{4}\left[a^3\,(1+\alpha)^3\right] \tag{2}$$

and

$$c_{Pu} = \frac{y}{V_m} = \frac{4\,y}{\left(A_1 + B_1\,y\right)^3\,(1+\alpha)^3\,\mathcal{N}} \tag{3}$$

Simple fitting functions are mentioned in literature [11] in order to reduce interdiffusion profile noise. They can be tested in order to extract solely volume interdiffusion from profiles where intergranular diffusion also occurs. The proposed functions assume that concentration data are antisymmetric with respect to their inflexion point:

$$c(x) = 0.25\,(\tanh(x) + 2) \tag{4}$$
$$c(x) = 0.75 - 0.5\,exp^{(-0.3x)^3} \tag{5}$$
$$c(x) = 0.5 + \left(3.49 \cdot 10^{-3}\,tan^{-1}(x)\right) \tag{6}$$

$$c(x) \quad = 0.75 - 0.25 \, erfc \left(\frac{x}{4 \, \widetilde{D} \, \Delta t} \right) \tag{7}$$

B.Messerschmidt [12] has carried out analytical fittings in order to facilitate the computation of $\widetilde{D}$ *vs.* c, expanding c as a polynomial in x:

$$c(x) \quad = \sum_{i=0}^{N} c_i \, x^i \tag{8}$$

S.Mendez both to suppress noise and extract volume diffusion coefficient from polycrystalline materials in the case of small diffusion coefficients used [13]:

$$c(x) \quad = \frac{1 - exp^{(-\lambda_1 \, x)}}{1 - \lambda_2 \, exp^{(-\lambda_1 \, x)}} \tag{9}$$

The first four of them show a major limitation because they are well suited only for an antisymmetric curve (relatively to its inflexion point). Messerschmidt method is well suited only for the study of the plateaus of the interdiffusion profiles. The last one (S. Mendez's work) does not make these assumptions, but implicitly makes the hypothesis that the origin has been taken far enough from the interface so that the concentration slope can be considered as equal to 0. An advantage of S.Mendez's fitting function is that it can handle interdiffusion profile data with very small diffusion coefficients using large values of λ_1 and λ_3.

In this work the following function has been used:

$$c(x) = \lambda_1 - \lambda_2 \frac{1 - \lambda_3 \, exp^{-\lambda_4 \, x}}{1 + \lambda_5 \, exp^{-\lambda_4 \, x}} \tag{10}$$

with a set of parameters $\lambda_i > 0 \quad i \in \{1, \dots, 5\}$ which can be different for x smaller or greater than the inflexion point abscissa x_0 and denoted by l and r subscripts for left and right hand side respectively. $ln(\lambda_5)$ and $ln(\lambda_3)$ are preferred to λ_5 and λ_3 for numerical handling in software when the diffusion coefficients are very small to avoid computational precision loss. The smaller the diffusion coefficient is, the higher the values of λ_3 and λ_5 are and intermediate values during computation may exceed machine storage representation.
Parameters for the left and right hand side of the function are linked by the

continuity of the function, which holds in the case of a solid solution but which may not be the case if a demixtion occurs at the interface, as well as by the continuity or not of the first derivative of the concentration. This derivative might not be continuous if the interdiffusion mechanism changes with composition (e.g. if the interdiffusion profile runs through two different phases). In that case a discontinuity of $\widetilde{D}$ can be balanced by a discontinuity of the derivative of the concentration. Thus, there is an advantage expressing $c(x)$ in terms of λ_1, λ_2, x_0 , $c(x_0)$ and $c'(x_0)$ for the continuous derivative case,

$$\lambda_3 = -\frac{2\,x_0\,c'(x_0)}{c(x_0)+\lambda_2-\lambda_1}\left(1-\frac{2\,(\lambda_1-c(x_0))}{\lambda_2}\right) \tag{11}$$

$$\lambda_4 = -\frac{2\,c'(x_0)}{c(x_0)+\lambda_2-\lambda_1} \tag{12}$$

$$\lambda_5 = -\frac{2\,x_0\,c'(x_0)}{c(x_0)+\lambda_2-\lambda_1} \tag{13}$$

whereas when the first derivative of the concentration is discontinuous at the inflexion point $c(x)$ can be expressed in terms of λ_1, λ_2, λ_4, x_0 and $c(x_0)$:

$$\lambda_3 = \left[1-2\,\frac{(\lambda_1-c\,(x_0))}{\lambda_2}\right]e^{x_0\,\lambda_4} \tag{14}$$

$$\lambda_5 = e^{x_0\,\lambda_4} \tag{15}$$

λ_i are meaningful, their value is linked to the maximum and minimum values of the concentration c along the profile (resp. c^+ and c^-):

$$\lim_{x\to-\infty} c(x) = \lambda_{l1} + \frac{\lambda_{l2}\,\lambda_{l3}}{\lambda_{l5}} = c^- \tag{16}$$

$$\lim_{x\to+\infty} c(x) = \lambda_{r1} - \lambda_{r2} = c^+ \tag{17}$$

Expressing (10) in terms of $\lambda_{1l},\lambda_{2l},x_0,c\,(x_0),c'\,(x_0),\lambda_{1r},\lambda_{2r}$ can be of interest in the case of continuity of the derivative at the inflexion point:

$$c\,(x) = \left(\lambda_1 - \frac{\lambda_2 - (2\,f\,(x_0)+\lambda_2-2\,\lambda_1)\,e^{\frac{2\,f'(x_0)\,(x-x_0)}{f(x_0)+\lambda_2-\lambda_1}}}{e^{\frac{2\,f'(x_0)\,(x-x_0)}{f(x_0)+\lambda_2-\lambda_1}}+1}\right) \tag{18}$$

in that case the parameters are denoted m_i hereafter. Some features of these

i	m_i (continuous case)	m_i (discontinuous case)
1	λ_{l1}	λ_{l1}
2	λ_{l2}	λ_{l2}
3	x_0	λ_{l4}
4	$c\left(x_0\right)$	x_0
5	$c'\left(x_0\right)$	$c\left(x_0\right)$
6	λ_{r1}	λ_{r1}
7	λ_{r2}	λ_{r2}
8	not applicable	λ_{r4}

Table 1: Meaning of m_i parameters for the two fitting cases

functions make them convenient tools for diffusion studies:
- their derivatives are negative (for $\lambda_i > 0$) and tend towards 0 in $\pm\infty$:

$$\frac{dc}{dx} = -\frac{\lambda_2\,\lambda_4\,\left(exp^{ln(\lambda_3)-\lambda_4\,x} + exp^{ln(\lambda_5)-\lambda_4\,x}\right)}{(exp^{ln(\lambda_5)-\lambda_4\,x}+1)^2} \tag{19}$$

$c(x)$ has to be monotoneous ($\frac{dc}{dx} < 0$), otherwise the direction of the flux would change along the interdiffusion profile.

$$\lim_{+\infty}\frac{dc}{dx} = \lim_{-\infty}\frac{dc}{dx} = 0 \tag{20}$$

This is required for interdiffusion so that when concentration is that of the initial materials (*i.e.* $c = cst = c^+$ or c^- at $x \to \pm\infty$) $\frac{dc}{dx} = 0$ and the flux is nul.
Two of their properties are of interest for the use of both Boltzmann-Matano and den Broeder methods as it will be described in sections 3 and 4 respectively:
- they possess a reciprocal function with an analytical expression:

$$x(c) = \frac{\ln\left(\frac{\lambda_2\,e^{\ln(\lambda_3)-\ln(\lambda_5)}}{c+\lambda_2-\lambda_1} - \frac{c-\lambda_1}{c+\lambda_2-\lambda_1}\right) + \ln(\lambda_5)}{\lambda_4} \tag{21}$$

- the function $g(x) = x\,\frac{dc}{dx}$ has got primitives, let denote P the one which is $\frac{\lambda_2\,Ln(\lambda_5)\left(e^{Ln(\lambda_3)-Ln(\lambda_5)}+1\right)}{\lambda_4}$ at $-\infty$:

$$\begin{aligned}P(x) \quad &= \quad \frac{\lambda_2\left(e^{ln(\lambda_3)-Ln(\lambda_5)}+1\right)\left(Ln\left(e^{\lambda_4\,x-Ln(\lambda_5)}+1\right)+Ln(\lambda_5)\right)}{\lambda_4}\\ &\quad - \quad \frac{\lambda_2\left(e^{Ln(\lambda_3)-Ln(\lambda_5)}+1\right)x\,e^{\lambda_4\,x}}{e^{\lambda_4\,x}+\lambda_5}\end{aligned} \tag{22}$$

The existence of such analytical functions simplifies a lot the numerical estimation of $\widetilde{D}$ vs. c.

A more mathematical approach consisting in expanding the solution of the second Fick law on a basis of erf functions has been developed by A.G. Nikitin [14], however this method also requires both to find the set of coefficients from the experimental data (deconvolution) and then to numerically rebuild $\widetilde{D}$ vs. c. Handling a simple function as the one proposed in this work is easier.

2.3. Extracting volume diffusion profiles

Experiments provide profiles acquired by means of an Electron Probe MicroAnalyser (EPMA) which are due both to volume and faster grain-boundary diffusion phenomena. In the case where material grains are large enough, the contribution of grain-boundary diffusion may be substracted by keeping along the profile the only points which pertain to the bulk of grains. Since the microstructure (grain boundaries) may not have been revealed by a chemical or thermal etching, a way of selecting "good" points would be to keep only local maxima for $c < c(x_0)$ and local minima for $c > c(x_0)$. A way of automatizing such a procedure is to give a weight w_i to each point (x_i, c_i), $i \in \{0, \ldots, n\}$ smaller when the concentration is too low below the current smoothed curve (the one of the current iteration k) on the left side of the curve and smaller when the concentration is too high above this same curve on the right side of the inflexion point.

A Hooke and Jeeves procedure [15] has been used in order to minimize the test function:

$$\chi_k^2 = \sum_{i=0}^{n} w_{k_i} \left(c_i - c\left(x_i \right) \right)^2 \tag{23}$$

with

$$w_{k_i} = 10^{-3} \, w_{0_i} \left| 1 - \frac{contrib\_\chi^2{}_{k-1}}{\chi_{k-1}^2} \right|^p \tag{24}$$

where w_{0_i} are the initial weights depending on the confidence associated with point #i (based on the discrepancy, for instance, between the sum over all elements of their weight percentage and 100%):

$$w_{0_i} = exp^{-\frac{1}{2} \left(\frac{100 - \sum_{e=1}^{n \, el.} w_e}{\sigma_w} \right)^2} \tag{25}$$

where σ_w is the uncertainty upon the sum over the weight percent of the elements.

$contrib\_\chi^2{}_{k-1}$ is defined by:

$$contrib\_\chi^2{}_{k-1} = \frac{w_{k-1_i}\,(c_i - c\,(x_i))^2}{\chi^2_{k-1}} \qquad (26)$$

The parameters for the Hooke and Jeeves method are the m_i.

This method has been used on a $UO_2/U_{1-y}Pu_yO_{2-z}$ polycrystalline sample. Figure 1 gives the raw and fitted concentration curves for $\lambda_{l\,1} = 0.033\,mol.\,cm^{-3}$, $\lambda_{l\,2} = 0.0063\,mol.\,cm^{-3}$, $x_0 = 572.5\,\mu m$, $c\,(x_0) = 0.0336\,mol.\,cm^{-3}$, $c'\,(x_0) = -0.0003375\,mol.\,cm^{-3}.\mu m^{-1}$, $\lambda_{r\,1} = 0.0317\,mol.\,cm^{-3}$ and $\lambda_{r\,2} = 0.0093\,mol.\,cm^{-3}$, so that $\lambda_{3l} = 3.63785 \cdot 10^{+22}$, $\lambda_{5g} = 2.78188 \cdot 10^{+22}$, $\lambda_{3r} = 9.71611 \cdot 10^{+15}$, $\lambda_{5r} = 7.59326 \cdot 10^{+15}$.

A drawback of the method is the need to find a set of parameters close enough to the one which leads to a minimum in χ^2 in order to converge. However it is not a strong constraint since equations (11), (13), (16) and (17) help assigning first values to λ_i.

An advantage of this method is to give the uncertainties upon the seeked parameters which are the values of the search steps in each direction (one direction per parameter) when χ^2 stops decreasing.

2.4. Uncertainty upon c

2.4.1. Limits of EPMA for very small interdiffusion coefficients: a source of uncertainty

Uncertainties can be assigned to EPMA measurements using ISO/GUM recommandation [16]. Both, physical phenomena following Poisson law (X-Ray emission of the probed volume) and other key factors under study in the measurement process regarded as corrections (ZAF, surface roughness...) are taken into account:

$$w_{Spl} = \frac{\left(\dfrac{N_{Spl}}{t_{Spl}} - \dfrac{N_{bckgd_{Spl}}}{t_{bckgd_{Spl}}}\right)}{\left(\dfrac{N_{std}}{t_{std}} - \dfrac{N_{bckgd_{std}}}{t_{bckgd_{std}}}\right)}\, w_{std}\, c_{ZAF}\, c_{inhom.}\, c_{roughness}\, c_{n.m.el.} \qquad (27)$$

where Spl stands for sample, w_{Spl}: weight percent of the measured element in the sample, N_{Spl}: count number due to the sample, t_{Spl}: time of acquisition for the sample, $bckgd$: background, std: standard, w_{std}: the weight
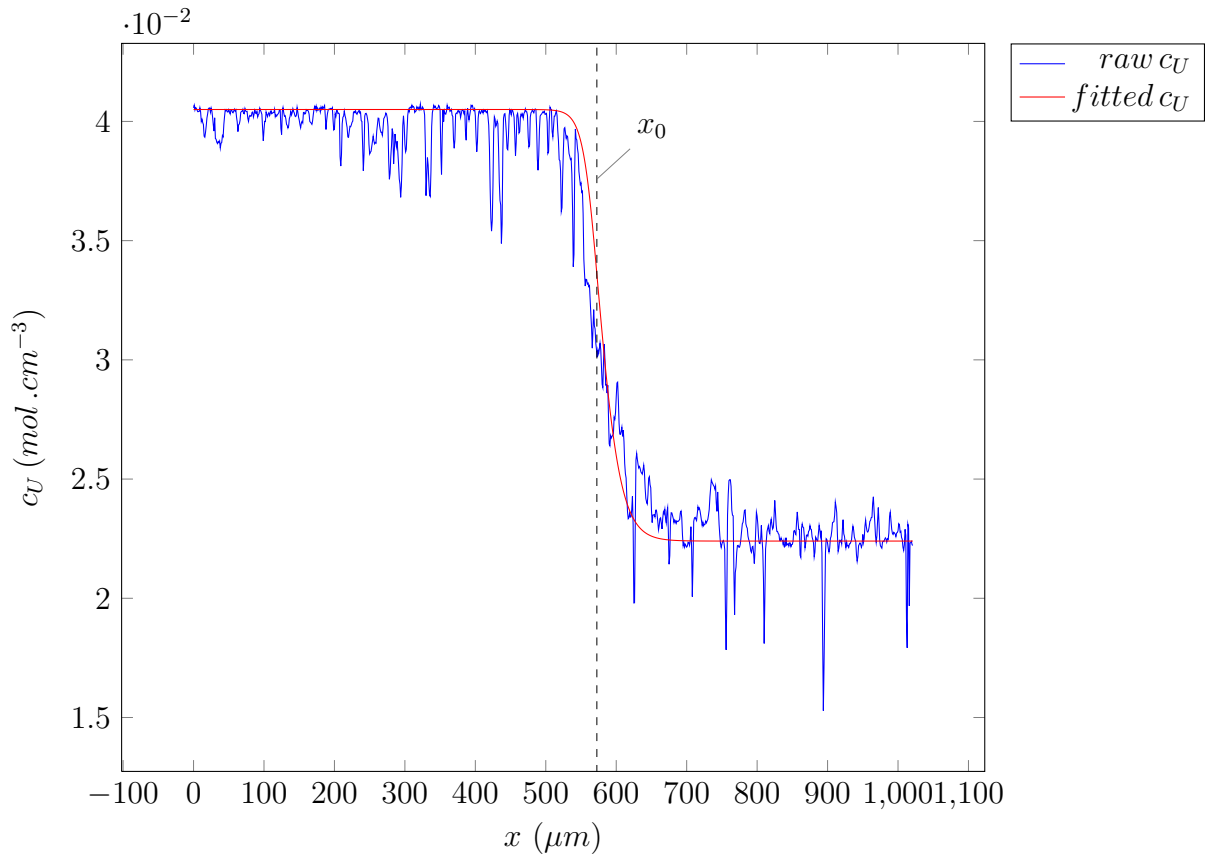
Figure 1: raw and fitted concentrations for $\lambda_{l\,1}$ = $0.033\,mol\,.cm^{-3}$, $\lambda_{l\,2}$ = $0.0063\,mol\,.cm^{-3}$, x_0 = $572.5\,\mu m$, $c\,(x_0)$ = $0.0336\,mol\,.cm^{-3}$, $c'\,(x_0)$ = $-0.0003375\,mol\,.cm^{-3}.\mu m^{-1}$, $\lambda_{r\,1}$ = $0.0317\,mol\,.cm^{-3}$ and $\lambda_{r\,2}$ = $0.0093\,mol\,.cm^{-3}$ $\left(\lambda_{3l} = 3.63785 \cdot 10^{+22}, \lambda_{5g} = 2.78188 \cdot 10^{+22}, \lambda_{3r} = 9.71611 \cdot 10^{+15}, \lambda_{5r} = 7.59326 \cdot 10^{+15}\right)$.

percent of the measured element in the standard, c_{ZAF}: ZAF correction, $c_{inhom.}$: correction due to the inhomogeneity of the material, $c_{roughness}$: correction due to the roughness of the sample, $c_{n.m.el.}$: correction due to non measured elements. Main of the uncertainty causes aforementioned generally lead to very small corrections, except in the case of interdiffusion, the inhomogeneity inherent to the diffusion phenomenon itself. In the same manner as raw EPMA measurements can be corrected by a factor $c_{inhomog.}$ due to the inhomogeneity of the sample, the interdiffusion profile $c(x)$ expressed in terms of the concentration of an element ($mol\,.cm^{-3}$) can be corrected by an analog correction $c'_{inhomog.}$. In this work the diffusion contribution to $c'_{inhom.}$ has been analysed. Figure 2 represents the axis of the acquisition line along which measurements were carried out as well as the interface of the materials.

For simplicity the measurement volume of the microprobe is supposed to be a sphere of radius $R = 0.5\mu m$. If the acquisition line is orthogonal to the interface and $\bar{c}$ denotes the value of c measured by the microprobe,

$$\bar{c}\left(x_i\right) = \frac{3}{4\,R^3} \int_{x_i-R}^{x_i+R} \left(R^2 - \left(x - x_i\right)^2\right)\,c(x)\,\mathrm{d}x \qquad (28)$$

where $c(x)$ is given by (18). As a matter of fact the measured value of concentration which is fitted is already an averaged one: c cannot be measured only $\bar{c}$ can. In order to evaluate the real point value of this function ($c(x)$) several acquisitions would be needed with a varying starting point. This cannot be the case with the EPMA sample holder the position of which can only be shifted by 1 μm along two perpendicular directions and the process would however be too time consumming. Evaluation of the impact of this averaging effect is carried out on the measured concentration $\bar{c}$ instead, assuming that:

$$c - \bar{c} \approx \bar{c} - \bar{\bar{c}} \qquad (29)$$

with $\bar{\bar{c}}$ the average of the measured $\bar{c}$ concentration. This should not be too rough an approximation as far as these differences remain small.
In order to be able to measure very small diffusion coefficients the acquisition line makes a very small angle α with respect to the interface. Let Y_i be the orthogonal projection of the point of abscissa x_i along the acquisition line onto the Y axis (perpendicular to the interface in the plane defined by the probed surface of the sample) and $c^{\perp}\left(Y_i\right)$ the concentration in the plane the
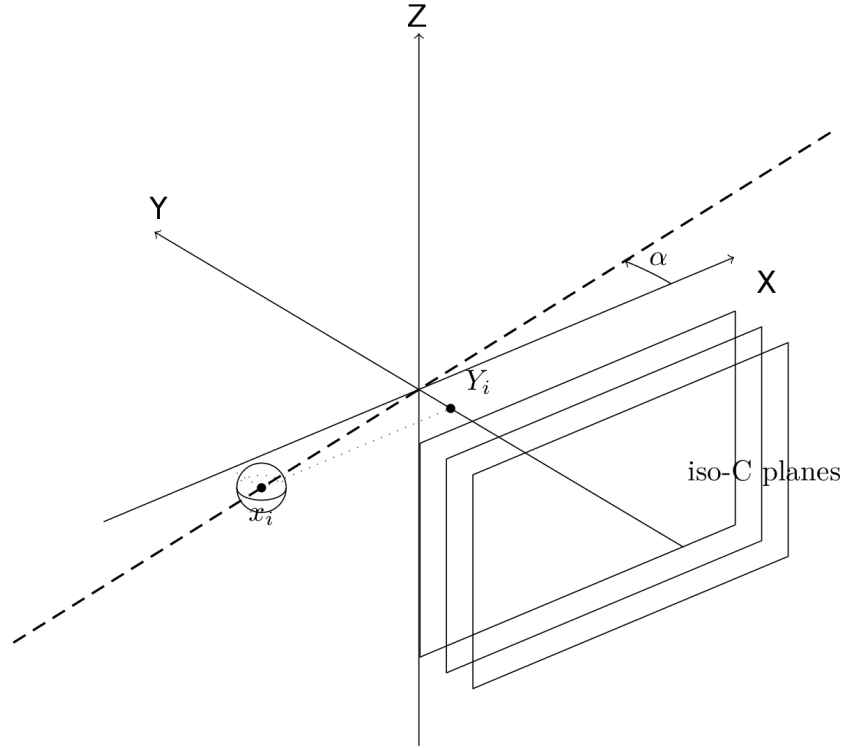
Figure 2: EPMA acquition line on top of the sample (with iso-concentration planes)

equation of which is $Y = cst = Y_i$.

$$
\begin{aligned}
c^\perp (Y) &= c_{\lambda_1, \lambda_2, \lambda_3, \lambda_4, \lambda_5} \left(\frac{Y}{sin(\alpha)} + x_i \right) \\
&= c_{\lambda_1, \lambda_2, \lambda_3\, e^{-\lambda_4\, x_i}, \frac{\lambda_4}{sin(\alpha)}, \lambda_5\, e^{-\lambda_4\, x_i}} (Y)
\end{aligned}
\tag{30}
$$

$\bar{c}(x_i)$ becomes:

$$
\begin{aligned}
\bar{c}(x_i) &= \overline{c^\perp}(Y_i) \\
&= \frac{3}{4\,R^3} \int_{Y_i - R}^{Y_i + R} \left(R^2 - (Y - Y_i)^2 \right) c_{\lambda_1, \lambda_2, \lambda_3\, e^{-\lambda_4\, x_i}, \frac{\lambda_4}{sin(\alpha)}, \lambda_5\, e^{-\lambda_4\, x_i}} (Y)\, \mathrm{d}Y
\end{aligned}
\tag{31}
$$

The closer to the interface the iso-concentration planes are, the narrower they are one from each other for a constant concentration step. Thus, it can
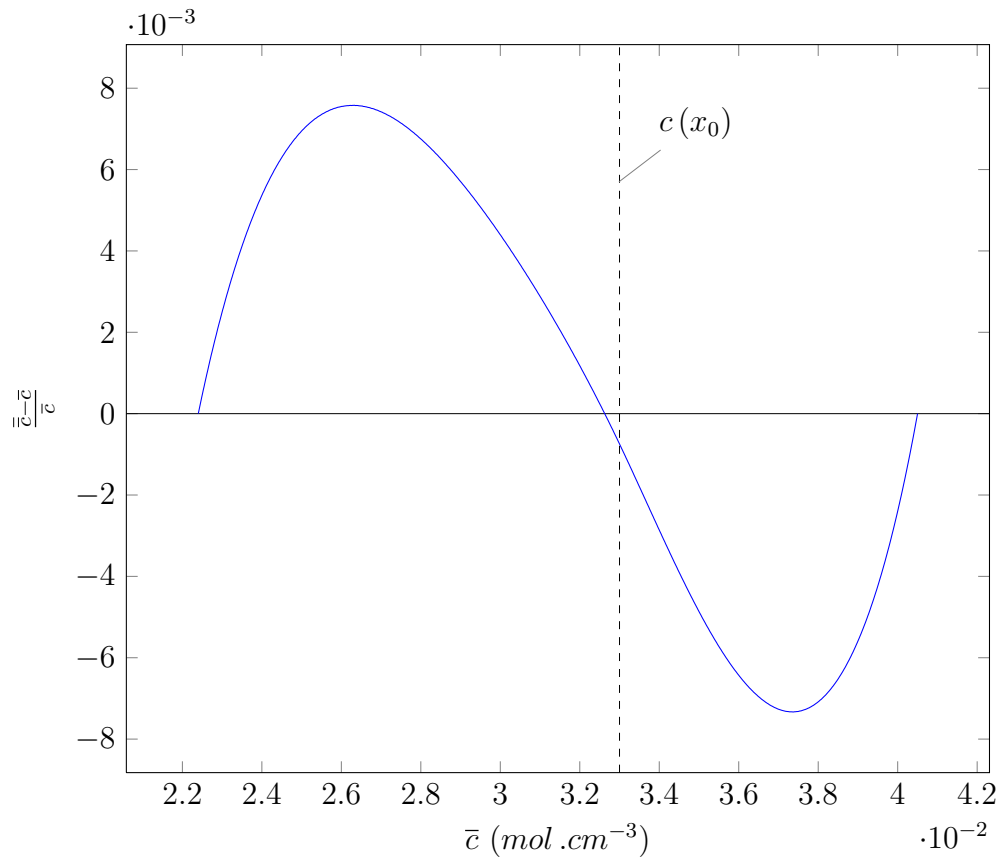
Figure 3: Averaged EPMA concentration $\bar{\bar{c}}$ and EPMA concentration $\bar{c}$ versus $\bar{c}$

be expected that the averaging effect of the measurement is greater near the interface where $\left\|\overrightarrow{\nabla}c\right\|$ is high except at the inflexion point if the profile is antisymmetric (both side contributions annihilate).

Figure 3 gives the relative difference between $\bar{\bar{c}}$ and $\bar{c}$. In the following c notation is used instead of $\bar{c}$.

2.4.2. Uncertainty upon x

Uncertainty upon the x coordinate along the profile has been evaluated taking into account several points:

- the surface of the sample may not be parallel to the sample-holder plane,
- the surface of the sample may not be a plane,
- the material may have a high thermal expansion coefficient so that dis-

tances between two points when the EPMA measurement is done may be much shorter than the distance between these same points at the temperature of the experiment.

Despite efforts made to smoothen the sample surface prior to EPMA analysis, on a millimeter scale (*i.e.* interdiffusion profile length), the surface of the sample may not be a plane. Or, even for a perfectly planar sample, its plane may not be perfectly parallel to the sample-holder surface. The equation of the mean plane of the sample surface in the axis of the microprobe is obtained as follow. The three coordinates relatively to the sample-holder axis system of each acquisition point along a profile, as well as those of at least two extra reference points, e.g. these denoted A and B in Figure 4 are used for the determination of the mean least-square plane. In the case of
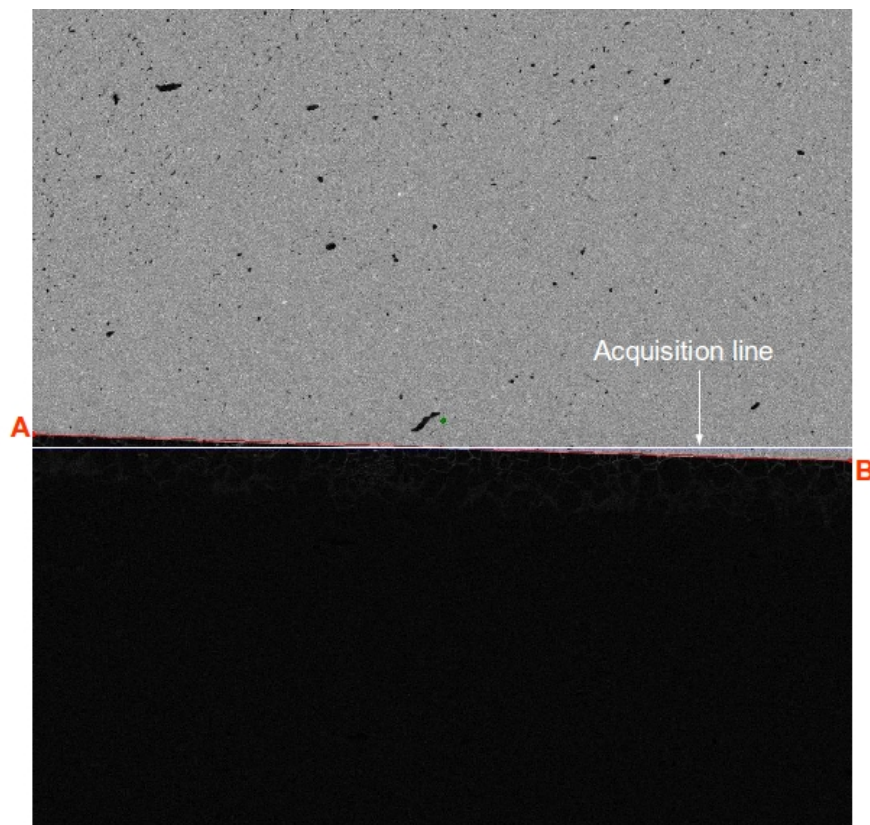

Figure 4: EPMA Pu X map with an acquisition line and the two points A and B at each end of the interface

several acquisition profiles in the same area of the material points from all the profiles are taken into account. The initial points are projected onto this plane and then projected onto a least-square line in the projection plane. Least-square uncertainties upon these coordinates are then calculated. A subsequent correction is done along a profile on the basis of the Pu weight content and on the stoichiometry (deduced from Pu weight content, temperature and oxygen potential) and temperature in order to compute a thermal expansion coefficient and correct point spacing along an acquisition profile. In the case of our materials, and in the specific thermodynamic conditions used (composition, temperature, oxygen potential), the overall correction, obtained as the uncertainties associated to the least square fitting methods was close to $1/1000$ which means $u(x) \simeq 0.5 \mu m$ near the inflexion point x_0 (the first measurement point was chosen as the origin and the profiles have approximately 1000 points).

In the case of Boltzmann-Matano method (see section 3), this uncertainty is taken into account as the uncertainty upon x_0 and x_M, in the case of den Broeder method (see section 4) as the uncertainty upon x_0, whereas in the case of Hall method as that upon $x - x_M$ (see section 4.3).

2.4.3. Uncertainty upon c function

Uncertainty upon concentration function has got several origins,
- the acquisition technique (here the EPMA), its limitations have been described hereabove, its contribution on the uncertainty upon c is $u_{tech.}(c) = \delta c$,
- the choice of the fitting function: small variations in the value of parameters m_i can give acceptable values for the fitting curve, for the case of a concentration function $c(x)$ the derivative of which is continuous at the inflexion point the contribution to $u(c)$ reads:

$$
\begin{aligned}
u_{fitt.}(c)^2 = \ & \left(\frac{\partial c}{\partial \lambda_{l1}}\right)^2 u\left(\lambda_{l1}\right)^2 + \left(\frac{\partial c}{\partial \lambda_{l2}}\right)^2 u\left(\lambda_{l2}\right)^2 + \\
& \left(\frac{\partial c}{\partial x_0}\right)^2 u\left(x_0\right)^2 + \left(\frac{\partial c}{\partial c(x_0)}\right)^2 u\left(c\left(x_0\right)\right)^2 + \left(\frac{\partial c}{\partial c'(x_0)}\right)^2 u\left(c\left(x_0'\right)\right)^2 + \\
& \left(\frac{\partial c}{\partial \lambda_{r1}}\right)^2 u\left(\lambda_{r1}\right)^2 + \left(\frac{\partial c}{\partial \lambda_{r2}}\right)^2 u\left(\lambda_{r2}\right)^2
\end{aligned}
\tag{32}
$$

all these partial derivatives have been computed analytically from equation (18).

In order to express final $\widetilde{D}$ values versus the atomic ratio y of one cation of the interdiffusion species (here Pu), the relationship (34) between y, c and

z $(y = y(c, z))$ is used.

If U concentration is considered:

$$c_U = \frac{4(1 - y)}{(A_1 + B_1 y)^3 (1 + \alpha)^3 \mathcal{N}} \tag{33}$$

or Pu concentration:

$$c_{Pu} = \frac{4 y}{(A_1 + B_1 y)^3 (1 + \alpha)^3 \mathcal{N}} \tag{34}$$

in both cases it can be noticed that y is a root of a third degree polynomial depending on c and z values, and its uncertainty, $u(y)$, depends both on $u(c)$ and $u(z)$. $\frac{\partial y}{\partial c}$ and $\frac{\partial y}{\partial z}$ have been computed anatlytically according to the propagation linked to the third degree polynomial resolution method.

$$u(y)^2 = \left(\frac{\partial y}{\partial c}\right)^2 u(c)^2 + \left(\frac{\partial y}{\partial z}\right)^2 u(z)^2 \tag{35}$$

$u(c)$ is computed as afore mentioned.

It could sound surprising that y be computed from c if we refer to (2.2). In section (2.2) values of c and y are those at the experimental points whereas in this section their value are considered at any point x along the acquisition line whether it is at the same location of an experimental point or not and thus in this section y is deduced from c.

Thus, the third origin of uncertainty is the partial lack of knowledge of the chemical composition of the particular sample we used: both initial parts of the sample had been finely characterized but as the heat treatment was stopped at the end of the interdiffusion experiment the oxygen content information from EPMA was not quantitative enough all along the profile to be used and the oxygen content had to be calculated by means of a thermodynamic model using temperature, oxygen potential and Pu EPMA concentration profile.

Table 2 sums up the different uncertainties used for the example of our study.

3. Boltzmann-Matano volume interdiffusion coefficient $\widetilde{D}$

Although Boltzmann-Matano method is less used because of more recent advanced methods such as Sauer and Freise [17], Wagner [18], and den Broeder modifications, it remains a straightforward starting point to evaluate interdiffusion coefficients.

parameter	value	uncertainty
λ_{l1}	$0.033\,(mol\,.cm^{-3})$	0.001
λ_{l2}	$0.0063\,(mol\,.cm^{-3})$	0.0002
x_0	$572.5\,(\mu m)$	0.5
$c\,(x_0)$	$0.0336\,(mol\,.cm^{-3})$	0.0006
$c'\,(x_0)$	$-0.0003375\,(mol\,.cm^{-3}\mu m^{-1})$	0.0000025
λ_{r1}	$0.0317\,(mol\,.cm^{-3})$	0.001
λ_{r2}	$0.0093\,(mol\,.cm^{-3})$	0.0002
α	$0.03176(rd)$	0.00046
z	$computed$	0.013
λ_{l3}	$computed : 3.63785 \cdot 10^{+22}$	–
λ_{l5}	$computed : 2.78188 \cdot 10^{+22}$	–
λ_{r3}	$computed : 9.71611 \cdot 10^{+15}$	–
λ_{r5}	$computed : 7.59326 \cdot 10^{+15}$	–

Table 2: Parameter uncertainties set by the user in the studied example

3.1. Boltzmann-Matano method

According to Boltzmann-Matano method $\widetilde{D}$ expression is the following:

$$\widetilde{D}\,(c^*) = -\frac{sin^2(\alpha)}{2\,\Delta t}\frac{\int_{-\infty}^{x^*}(x-x_M)\frac{dc}{dx}\,dx}{\frac{dc}{dx}\big|_{x^*}} \tag{36}$$

where α is the angle between the acquisition line and the interface and Δt the duration of the interdiffusion experiment (in isothermal conditions). In this work the abscissa x_M of 'Matano plane', (the one crossed by an equal amount of matter one way and the other) can be expressed using $c(x)$ definition (18) and its properties:

$$\begin{aligned}
x_M \quad &= \frac{(c(x_0)+\lambda_{l\,2}-\lambda_{l\,1})\left(x_0+\frac{\log(2)\,(c(x_0)+\lambda_{l\,2}-\lambda_{l\,1})}{c'(x_0)}\right)}{c^--c^+}\\
&+\frac{(c(x_0)+\lambda_{r\,2}-\lambda_{r\,1})\left(x_0-\frac{\log(2)\,(c(x_0)+\lambda_{r\,2}-\lambda_{r\,1})}{c'(x_0)}\right)}{c^--c^+}
\end{aligned} \tag{37}$$

For $x < x_0$:

$$\int_{-\infty}^{x^*}(x-x_M)\,\frac{dc}{dx}\,dx = P\,(x^*,\lambda_{r\,i}) - x_M(c-c^+) \tag{38}$$

while for $x \geq x_0$:

$$\int_{-\infty}^{x^*} (x - x_M) \frac{dc}{dx}\, dx = P(x_0, \lambda_{r\,i}) + P(x^*, \lambda_{l\,i}) - P(x_0, \lambda_{l\,i}) - x_M(c - c^+)) \quad (39)$$

In any case:

$$\frac{dc}{dx}|_{x^*} = -\frac{\lambda_2\,\lambda_4}{e^{\lambda_4\,x^* - Ln(\lambda_5)} + e^{Ln(\lambda_5) - \lambda_4\,x} + 2} + \frac{\lambda_2\,\lambda_4}{\left(e^{\lambda_4\,x^* - Ln(\lambda_3)} + e^{Ln(\lambda_5) - Ln(\lambda_3)}\right)\left(e^{\lambda_4\,x^* - Ln(\lambda_5)} + 1\right)}$$
$$-\frac{\lambda_2\,\lambda_4\,e^{Ln(\lambda_3) - Ln(\lambda_5)}}{e^{\lambda_4\,x^* - Ln(\lambda_5)} + 1}$$

$$(40)$$

Figure 5 gives Boltzmann-Matano interdiffusion coefficient as a function of uranium concentration c_U. As concentration is close to its limits (c^-, c^+) the values of $\widetilde{D}$ obtained by Boltzmann-Matano method are abnormally high as c tends towards its limits c^+ and c^-. The uncertainty upon $\widetilde{D}$ is discussed hereafter.

3.2. Uncertainty upon Boltzmann-Matano interdiffusion coefficient

Such uncertainty assessment with a fitting function have already been carried out: B. Messerschmidt [12] had calculated an uncertainty upon $\widetilde{D}(c)$ on the basis of the polynomial expansion of $c(x)$ but with the aim of emphasizing the weakness of Boltzmann-Matano method in the plateau areas. J.F.Cornet used an iterative method [5].
The uncertainty upon $\widetilde{D}$ from Boltzmann-Matano method with our fitting function has been studied hereafter. Several sources of uncertainties have been considered and are described hereafter.

3.2.1. EPMA averaging effect

The averaging effect of the EPMA has already been described for concentration c. The same assumption as that of section 2.4.3 is made here:

$$|\delta\widetilde{D}| = |\widetilde{D}(c) - \widetilde{D}(\bar{c})| \approx |\widetilde{D}(\bar{c}) - \widetilde{D}(\bar{\bar{c}})| \quad (41)$$

which leads to a contribution to $u\left(\widetilde{D}\right)$:

$$u_{tech.}\left(\widetilde{D}\right) = \delta\widetilde{D} \quad (42)$$

Although $\int (x - x_M) \frac{dc}{dx}$ has got an analytical expression on the basis of $c_{\lambda_1, \lambda_2, \lambda_3, \lambda_4, \lambda_5}$, as well as $\frac{dc}{dx}$, it is not the case for analog expressions with $\bar{c}$.
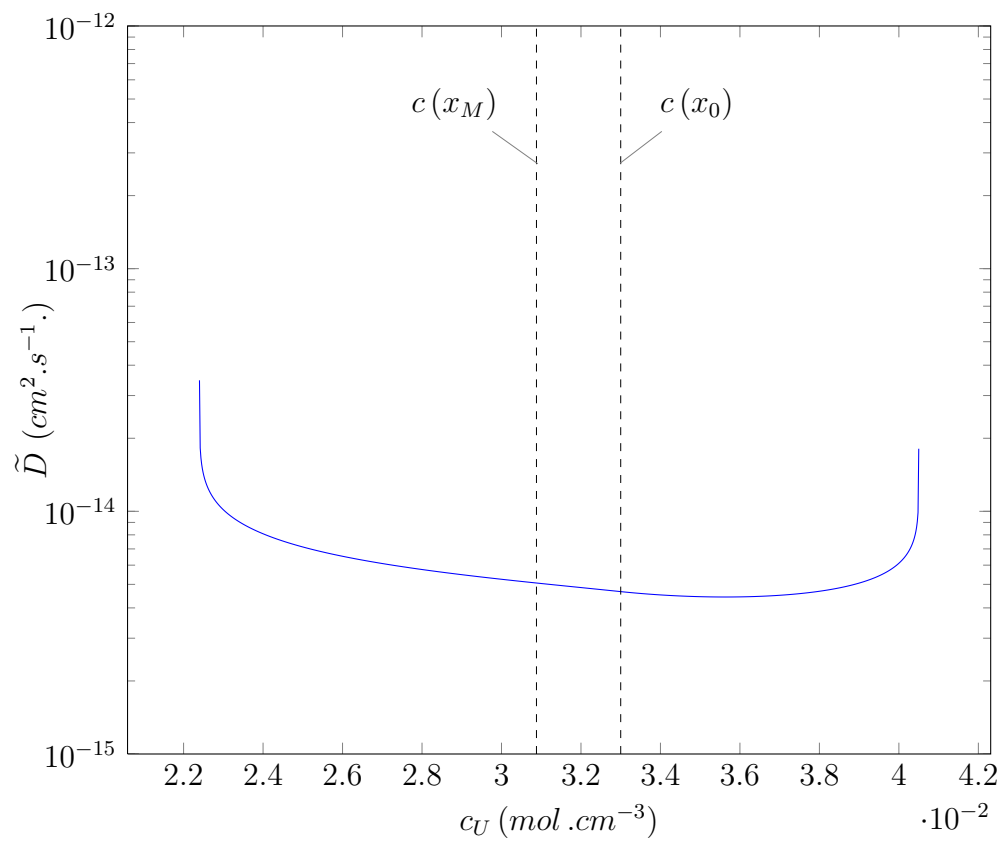
Figure 5: Boltzmann-Matano interdiffusion coefficient ($\widetilde{D}$) as a function of uranium concentration (c_U)

.

For this reason analog expressions related to $\bar{c}$ such as the integral in (31) can only be computed numerically. They have been evaluated by a Gauss-Legendre method with 24 points ξ_j in the reduced interval $[-1; 1]$.

$$
\begin{aligned}
\frac{d\bar{c}}{dx}\Big|_{Y_i} &= \frac{sin(\alpha)}{\frac{4}{3}R^3} \int_{Y_i-R}^{Y_i+R} (-2\,Y_i + 2\,Y)\, c_{\lambda_1,\lambda_2,\lambda_3\,e^{-\lambda_4\,x_i},\frac{\lambda_4}{sin(\alpha)},\lambda_5\,e^{-\lambda_4\,x_i}}(Y)\, \mathrm{d}Y \\
&= \frac{sin(\alpha)}{\frac{4}{3}R^3}\, R \sum_{j=1}^{24} w_j\, (-2\,Y_i + 2\,(R\,\xi_j + Y_i))\, c_{\lambda_1,\lambda_2,\lambda_3\,e^{-\lambda_4\,x_i},\frac{\lambda_4}{sin(\alpha)},\lambda_5\,e^{-\lambda_4\,x_i}}(R\,\xi_j + Y_i)
\end{aligned}
\tag{43}
$$

where ξ_i are Gauss-Legendre reduced abscissa and w_i their associated weights. Since the analog computation of $\widetilde{D}(\bar{c})$ is numeric its value may be slightly affected by the integration method, both $\widetilde{D}(c)$ and $\widetilde{D}(\bar{c})$ have been computated numerically as far as the evaluation of $|\widehat{D}(c) - \widetilde{D}(\bar{c})|$ was concerned. For this purpose $\int (x - x_M)\,\frac{dc}{dx}$ is approximated by means of a simple trapezium rule scheme, and $\frac{dc}{dx}$ by a simple forward finite differences method.

Since the uncertainty due to the averaging effect of the measurement technique (the main cause of EPMA uncertainty in our case) is of prime interest, it is compared to the value of the interdiffusion coefficient. Figure 6 shows the uncertainty upon $\widetilde{D}$ due to this averaging effect denoted δD versus concentration for our example ($\lambda_{l\,1} = 0.033\,mol\,.cm^{-3}$, $\lambda_{l\,2} = 0.0063\,mol\,.cm^{-3}$, $x_0 = 572.5\,\mu m$, $c(x_0) = 0.0336\,mol\,.cm^{-3}$, $c'(x_0) = -0.0003375\,mol\,.cm^{-3}.\mu m^{-1}$, $\lambda_{r\,1} = 0.0317\,mol\,.cm^{-3}$ and $\lambda_{r\,2} = 0.0093\,mol\,.cm^{-3}$). Hence, in this specific case, it can be concluded that in the studied range of U concentration EPMA averaging measurement process can be regarded as negligible leading to reliable values of $\widetilde{D}$ whereas for smaller interdiffusion coefficients other techniques may be required. For instance Rutherford Back Scattering (RBS) can be used if both parts of the interdiffusion couple are taken apart at the end of the experiment for analysis in the range $0.1\mu m$ up to $2\mu m$ [19] or, on a decreasing scale with tens nanometer resolution, Secondary Ion Mass Spectrometry (SIMS) can be applied [20] to analyse each separated part of the interdiffusion couple, or, with 1 nanometer resolution, coupled with Transmission Electron Microscopy (TEM) with high angle annular dark field (HAADF) imaging, Electron Dispersive Spectroscopy (EDS) and parallel electron energy loss spectroscopy (PEELS) [21] .

3.2.2. Uncertainty upon x_M

Uncertainty upon x_M value is taken into account, which is at the origin of the development of other methods such as den Broeder's method.

$$\begin{aligned}
u\left(x_M\right)^2 &= \delta^2 x_M + \\
&\left(\frac{\partial x_M}{\partial \lambda_{l1}}\right)^2 u\left(\lambda_{l1}\right)^2 + \left(\frac{\partial x_M}{\partial \lambda_{l2}}\right)^2 u\left(\lambda_{l2}\right)^2 + \\
&\left(\frac{\partial x_M}{\partial x_0}\right)^2 u\left(x_0\right)^2 + \left(\frac{\partial x_M}{\partial c(x_0)}\right)^2 u\left(c\left(x_0\right)\right)^2 + \left(\frac{\partial x_M}{\partial c'(x_0)}\right)^2 u\left(c\left(x'_0\right)\right)^2 + \\
&\left(\frac{\partial x_M}{\partial \lambda_{r1}}\right)^2 u\left(\lambda_{r1}\right)^2 + \left(\frac{\partial x_M}{\partial \lambda_{r2}}\right)^2 u\left(\lambda_{r2}\right)^2
\end{aligned}$$

(44)

Except for δx_M, analytical expressions have been used for the caculation of the partial derivatives $\frac{\partial x_M}{\partial m_i}$

In the case of the studied profile $u\left(x_M\right) = 0.5$ and $x_M = 576.3 \pm 0.5 \mu m$. This uncertainty leads to a contribution to the uncertainty upon $\widetilde{D}$:

$$u\left(\widetilde{D}\right) = \frac{\partial \widetilde{D}}{\partial x_M} u\left(x_M\right)$$

(45)

This effect is also given in Figure 6 and cannot be neglected as $c \to c^-$. A way of avoiding such a high uncertainty on this side of the concentration range would be for this half part of the domain $(c \geq c\left(x_M\right))$ to evaluate $\widetilde{D}$ by means of:

$$\widetilde{D}\left(c^*\right) = \frac{sin^2(\alpha)}{2\,\Delta t} \frac{\int_{x^*}^{+\infty}\left(x_M - x\right)\frac{dc}{dx}\,dx}{\frac{dc}{dx}\big|_{x^*}}$$

(46)

instead of (36).

3.2.3. Uncertainty upon α

$\widetilde{D}$ depends also on the angle α of the acquisition line with the interface: $\frac{\partial \widetilde{D}}{\partial \alpha} = 2\frac{cos(\alpha)}{sin(\alpha)}\widetilde{D}$. Although the choice of a small α angle leads to a high dependency of $\widetilde{D}$ on α, it has to be noticed that it increases the number of points in the vicinity of the interface, *i.e.* where concentration varies a lot and thus increases the precision upon $\lambda_{l1},...,\lambda_{r2}$. The number of significant points N_s (*i.e.* with a high weight because they influence greatly the shape of the curve $c = c(x)$) increases by a factor $\frac{1}{sin(\alpha)}$ and $u\left(m_i\right)_\alpha \propto \frac{1}{\sqrt{N_s^\alpha}} = \frac{\sqrt{sin(\alpha)}}{\sqrt{N_s^{\frac{\pi}{2}}}}$. In our example $\alpha = 0.033$, and $\frac{u(m_i)_{N_s^{\frac{\pi}{2}}}}{u(m_i)_{N_s^\alpha}} \simeq 5.5$ so that m_i parameters $(\lambda_{l1},...,\lambda_{r2})$ are

at least 5 times more precise than they would have been if deduced from the perpendicular profile.

This contributes to the uncertainty upon $\widetilde{D}$:

$$u\left(\widetilde{D}\right) = \frac{\partial \widetilde{D}}{\partial \alpha} u\left(\alpha\right) = 2 \cdot cotg\left(\alpha\right) \widetilde{D} \cdot u\left(\alpha\right) \tag{47}$$

$u\left(\alpha\right)$ is assessed on the basis of the uncertainty upon the least-square profile line and the uncertainty upon A and B location with respect to the interface of the materials. This contribution to $u\left(\widetilde{D}\right)$ is minimum as $\widetilde{D}$ reaches its minimum. This third effect is also represented in Figure 6 but remains smaller than 1/10 of the measured coefficient all along the profile.

3.2.4. Uncertainty upon m_i

$\widetilde{D}$ depends also directly on the parameters $\lambda_{l1},...,x_0,...,\lambda_{r2}$. Its partial derivatives $\frac{\partial \widetilde{D}}{\partial m_i}$ are calculated analytically once and are part of the software which has been developped.

Overall, $\widetilde{D}$ uncertainty reads:

$$
\begin{aligned}
u\left(\widetilde{D}\right)^2 &= \delta\widetilde{D}_y^2 + \frac{\partial \widetilde{D}}{\partial x_M}^2 u(x_M)^2 + \frac{\partial \widetilde{D}}{\partial \alpha}^2 u(\alpha)^2 + \frac{\partial \widetilde{D}}{\partial \lambda_{l1}}^2 u(\lambda_{l1})^2 + \frac{\partial \widetilde{D}}{\partial \lambda_{l2}}^2 u(\lambda_{l2})^2 + \\
&\quad \frac{\partial \widetilde{D}}{\partial x_0}^2 u(x_0)^2 + \frac{\partial \widetilde{D}}{\partial c(x_0)}^2 u(c\left(x_0\right))^2 + \frac{\partial \widetilde{D}}{\partial c'(x_0)}^2 u(c'\left(x_0\right))^2 + \\
&\quad \frac{\partial \widetilde{D}}{\lambda_{r1}}^2 u(\lambda_{r1})^2 + \frac{\partial \widetilde{D}}{\partial \lambda_{r2}}^2 u(\lambda_{r2})^2
\end{aligned}
\tag{48}
$$

Figure 7 gives the various relative contributions to $u\left(\widetilde{D}\right)$. For this particular case of study all parameter uncertainties have a nearly equal effect on $\widetilde{D}$ in the uranium composition range $[0.023; 0.0402] mol\,.cm^{-3}$. The most sensitive ones are the position of the inflexion point $(x_0, c\left(x_0\right))$ as well as the slope at this point $c'\left(x_0\right)$. However the contribution to $\widetilde{D}$ uncertainty $u\left(\widetilde{D}\right)$ turns out to be higher at each end of the diffusion profile. Contributions appear not to be symmetric with respect to the limits of the concentration interval simply reflecting the fact that the interdiffusion profile is not symmetric:

- $c\left(x_0\right) = 0.0336\,mol\,.cm^{-3} \neq \frac{c_- + c_+}{2} = 0.03145\,mol\,.cm^{-3}$,
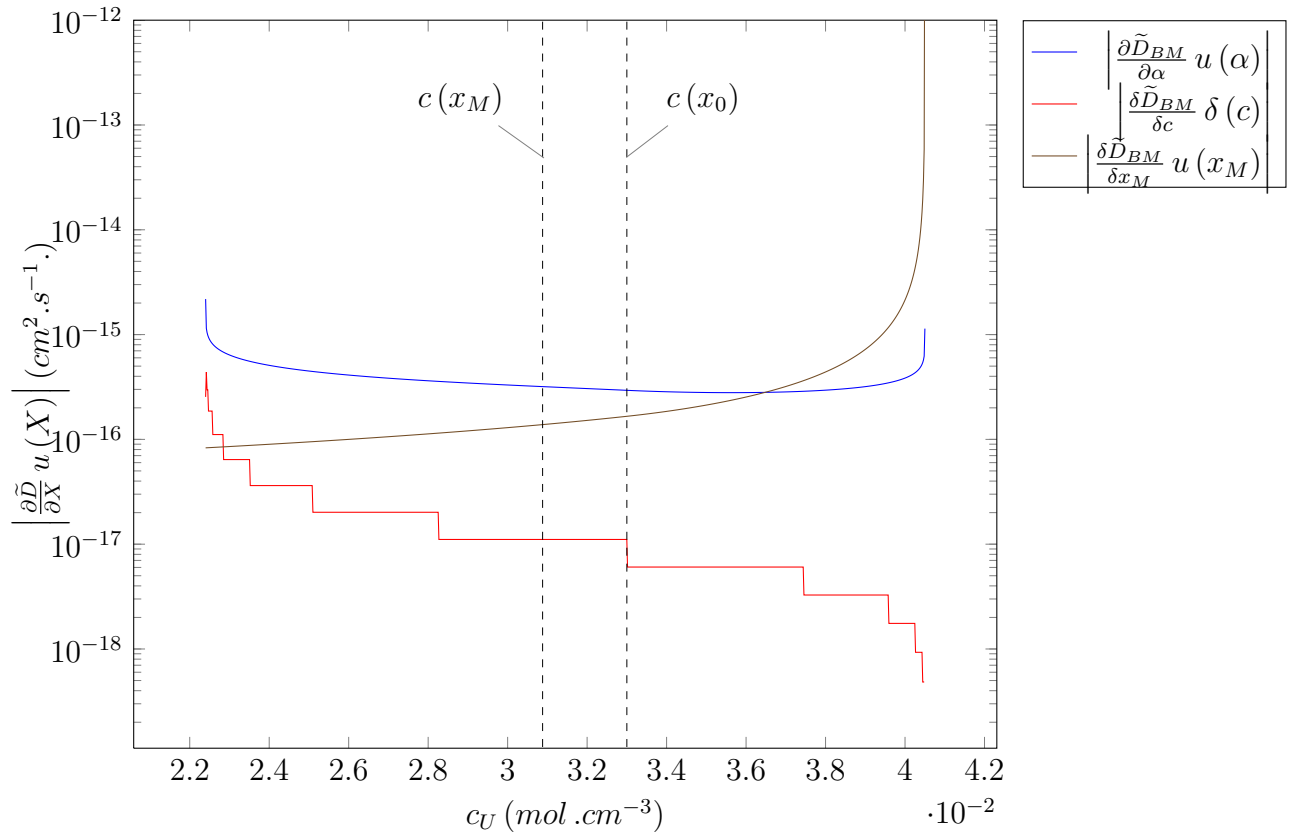- λ_{li} and λ_{ri} are not identical.

Figure 6: Contribution of the averaging effect of the Electron Probe MicroAnalyser (δc), of the uncertainty of the profile angle with the interface ($u(\alpha)$) and of Matano abscissa uncertainty ($u(x_M)$) to Boltzmann-Matano volume interdiffusion diffusion coefficient uncertainty for $\lambda_{l\,1} = 0.033\,mol\,.cm^{-3}$, $\lambda_{l\,2} = 0.0063\,mol\,.cm^{-3}$, $x_0 = 572.5\,\mu m$, $c(x_0) = 0.0336\,mol\,.cm^{-3}$, $c'(x_0) = -0.0003375\,mol\,.cm^{-3}.\mu m^{-1}$, $\lambda_{r\,1} = 0.0317\,mol\,.cm^{-3}$ and $\lambda_{r\,2} = 0.0093\,mol\,.cm^{-3}$
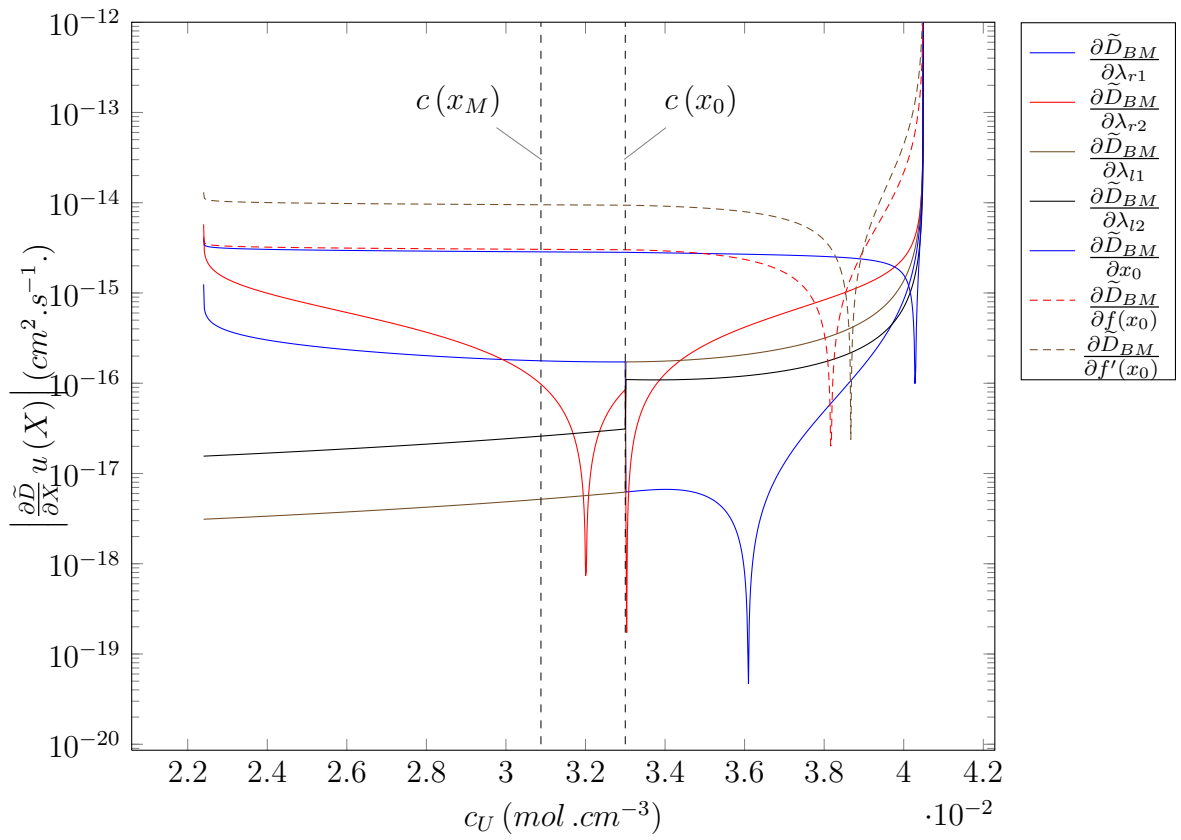
.

Figure 7: Contribution of uncertainties upon λ_{1l}, λ_{2l}, x_0, $c(x_0)$, $c'(x_0)$, λ_{1r} and λ_{2r} to Boltzmann-Matano interdiffusion coefficient

4. Den Broeder volume interdiffusion coefficient $\widetilde{D}$

Den Broeder method as been extensively used in the case of metals [22], [23] as well as ceramics [24]. The advantage of this method compared to Boltzmann-Matano method is mainly that it does not depend on the Matano abscissa and (to a lesser extent in our case) it can take into account atomic (or molecular) volume variations with concentration ([22],[23]).

4.1. Den Broeder method

In this method the interdiffusion coefficient is computed as a function of the atomic (or molecular in our case) ratio of one of the diffusing species N_2 and of its relative value Y. Let us say species #2 for instance. Then $\widetilde{D}$ reads:

$$\widetilde{D}\left(N_2^*\right) = \frac{\left(N_2^+ - N_2^-\right) V_m \left(N_2^*\right)}{2\,\Delta t \left(\frac{\partial N_2}{\partial x}\right)_{x=x^*}} \left[\left(1 - Y^*\right) \int_{-\infty}^{x^*} \frac{Y\,dx}{V_m} + Y^* \int_{x^*}^{+\infty} \frac{\left(1 - Y\right)\,dx}{V_m}\right] \tag{49}$$

This equation can be expressed in terms of $c(x)$ for which the analytical form defined by equation (18) is used here too. In this section $c(x)$ is denoted by $c_1(x)$ where 1 labels the species 1:

$$\widetilde{D}\left(c_1^*\right) = \quad \frac{-1}{c_1^- - c_1^+} \frac{1}{c_1\left(\frac{dV_m}{dx}\right)_{x=x^*} + V_m\left(\frac{dc_1}{dx}\right)_{x=x^*}}$$
$$\left[\left(c_1^- - c_1^*\right) \int_{-\infty}^{x^*} \left(c_1 - c_1^+\right) dx + \left(c_1^* - c_1^+\right) \int_{x^*}^{+\infty} \left(c_1^- - c_1\right) dx\right] \tag{50}$$

where c_1^- and c_1^+ are defined according to equations (16) and (17).
It is to be noticed that the discrete points used for the evaluation of all the terms are computed using the analytical expression of $c_1(x)$, which means that they can be chosen as close one to each other as needed.
The integrals in Den Broeder coefficient evaluation can be computed analytically. Since in the case of our material $\frac{dV_m}{dx}$ cannot be expressed analytically due to V_m expression (2), it has been computed by means of a Lagrange polynomial based derivation matrix with three point stencils, and the whole expression of $\widetilde{D}$ has been computated on a numerical basis. A simple trapezium rule was used for the determination of the integrals. Figure 8 gives den Broeder interdiffusion coefficient compared to that of Boltzmann-Matano. They are very close one to another.
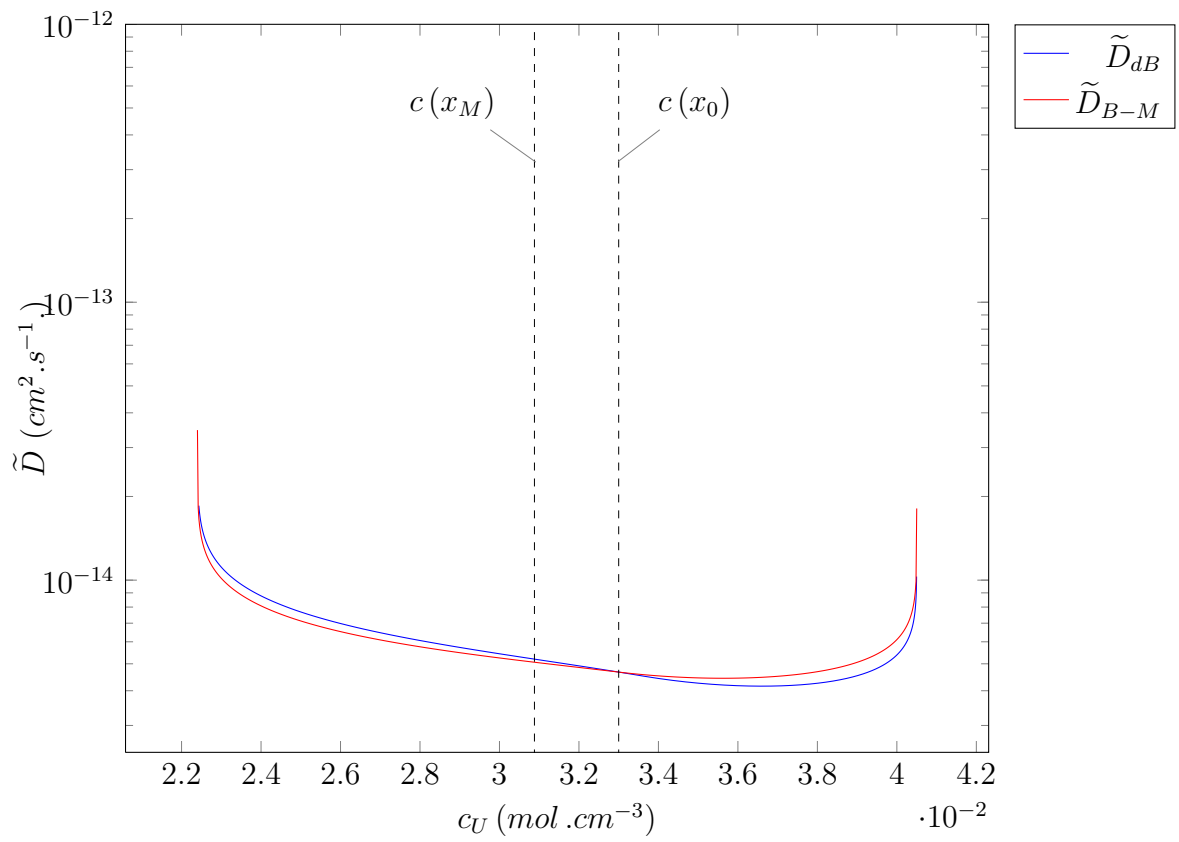
Figure 8: Den Broeder interdiffusion coefficient ($\widetilde{D}_{dB}$ blue) and Boltzmann-Matano interdiffusion coefficient ($\widetilde{D}_{B-M}$ red) as a function of uranium concentration (c_U)

.

4.2. Uncertainty upon Den Broeder interdiffusion coefficient

Since in our material applications the atomic ratio y is a meaningful parameter, $\widetilde{D}$ uncertainty has been estimated on the basis of the variables y and V_m (rather than c and V_m) and their contribution to $u\left(\widetilde{D}\right)$: $\delta\widetilde{D}_y$ which is the variation in $\widetilde{D}$ due to the uncertainty upon y (*i.e.* $u(y)$) and $\delta\widetilde{D}_{V_m}$ which is the uncertainty in $\widetilde{D}$ due to the uncertainty upon V_m.

$$u\left(\widetilde{D}\right)^2 = \delta\widetilde{D}_y^2 + \delta\widetilde{D}_{V_m}^2 + \left(\frac{\partial\widetilde{D}}{\partial\alpha}\right)^2 u\left(\alpha\right)^2 \tag{51}$$

$\delta\widetilde{D}_y$ (resp. $\delta\widetilde{D}_{V_m}$) is simply obtained by computing $\widetilde{D}$ using y and $y \pm u(y)$ (resp. $V_m \pm u\left(V_m\right)$). $u(y)$ is computed as described in section 2.4.3, *i.e.* as a function of $u(z)$ and $u(c)$, so that the influence of each parameter λ_1, λ_2, x_0, $c\left(x_0\right)$ and $c'\left(x_0\right)$ can be studied. The partial derivatives of the expression of the molar volume given in section 2.4.3 lead to the uncertainties upon V_m:

$$u\left(V_m\right)^2 = \left[\left(\frac{\partial V_m}{\partial z}\right)^2 u(z)^2 + \left(\frac{\partial V_m}{\partial y}\right)^2 u(y)^2\right] \tag{52}$$

Thus, $\widetilde{D}$ uncertainty in den Broeder method is built up of the same terms as for Boltzmann-Matano method, without $\frac{\partial\widetilde{D}}{\partial x_M}u\left(x_M\right)$ term but with an extra $\frac{\partial\widetilde{D}}{\partial V_m}u\left(V_m\right)$ which remains smaller.

Despite the higher uncertainty of Boltzmann-Matano method due to x_M, on our example both methods give identical results. This is mainly due to the choice of the fitting function which has lead to analytical expressions for the Boltzmann-Matano method. As concentration comes closer to its plateau values (c^- and c^+) on each side of the interfaces, den Broeder or Boltzmann-Matano methods are not precise enough to be used, instead Hall method is preferred. The different sources of uncertainties are given in Figure 9. This method is commonly used in conjonction with both of these methods in order to estimate $\widetilde{D}$ *vs.* c on the whole concentration range (Boltzmann-Matano method in conjonction with Hall method: in the case of uranium and plutonium interdiffusion [25], or in the case of Ti and a Mo-alloy interdiffusion [26], den Broeder method in conjonction with Hall method: in the case of Ge in nickel alloys [27], Ti-Mo interdiffusion [28], or carbon diffusion in ferritic steels [29]).
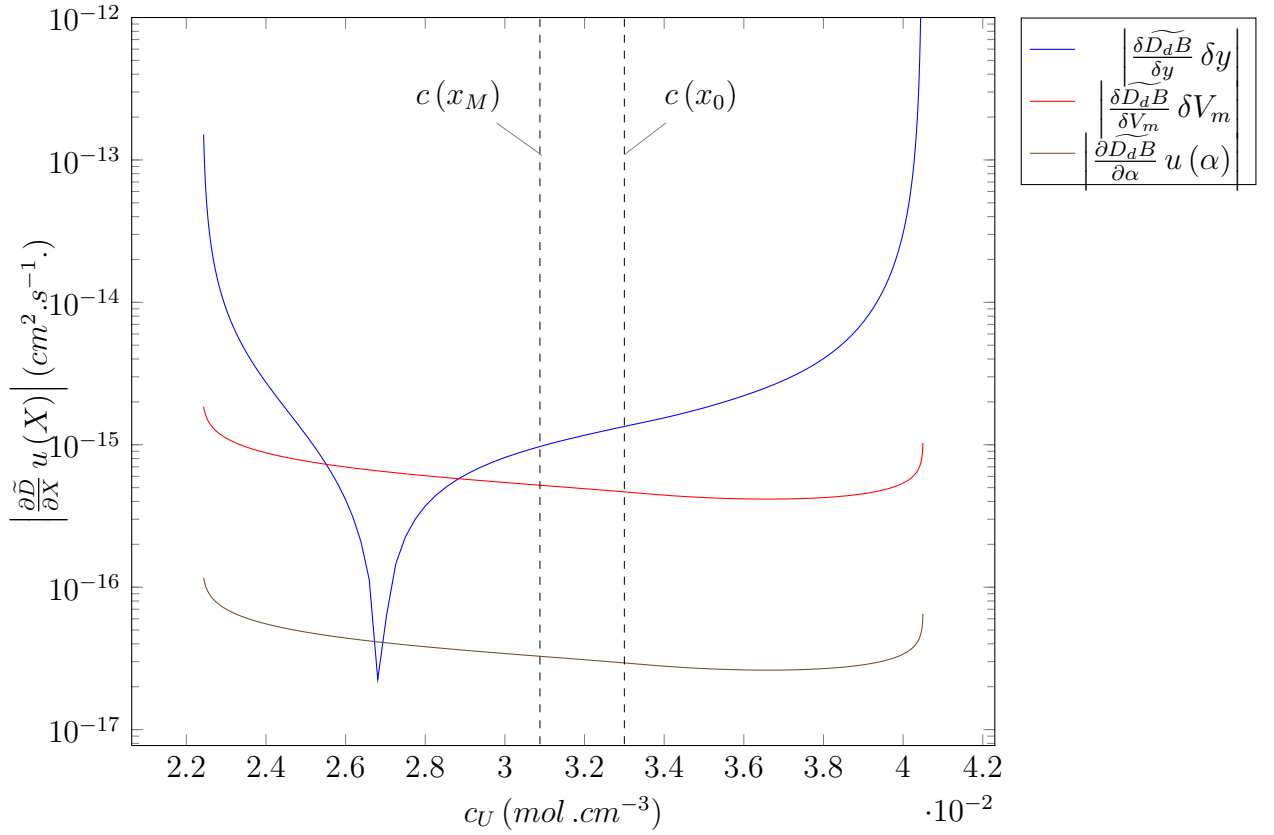
Figure 9: Contribution of y, Vm and α uncertainties upon Den Broeder interdiffusion coefficient as a function of uranium concentration (c_U)

.

4.3. Hall method

In this section too, the discrete points used are generated as close as needed one to each other by means of the analytical form of $c(x)$ given by equation (18).

The relative atomic ratio Y is defined by: $Y = \frac{c - c_{min}}{c_{max} - c_{min}}$ and U by $U = erf^{-1}(2Y - 1)$. As $c \to c_{min}$ (resp. c_{max}), U versus $\frac{x - x_M}{\sqrt{\Delta t}}$ becomes a straight line: $U \to \frac{(x - x_M)h_-}{\sqrt{(\Delta t)}} + k_-$ (resp. $U \to \frac{(x - x_M)h_+}{\sqrt{(\Delta t)}} + k_+$).

For the side of the curve left to the inflexion point (decreasing concentration

profile) $\widetilde{D}$ reads:

$$\widetilde{D}_- = \frac{1}{4\,h_-^2} \left[1 - k_-\,\sqrt{\pi}\,exp^{U^2}\,(1 - erf(U)) \right] \tag{53}$$

with $\lim_{x\to-\infty} \widetilde{D}_- = \frac{1}{4\,h_-^2}$ and on the right hand side:

$$\widetilde{D}_+ = \frac{1}{4\,h_+^2} \left[1 + k_+\,\sqrt{\pi}\,exp^{U^2}\,(1 + erf(U)) \right] \tag{54}$$

with $\lim_{x\to+\infty} \widetilde{D}_+ = \frac{1}{4\,h_+^2}$.

k_-, h_-, k_+ and h_+ are obtained by fitting the asymptots of the interdiffusion profile U vs. $\frac{x-x_M}{\sqrt{\Delta t}}$ (i.e. on each side, q% of the concentration interval $\left[c_{min}; c_{min} + \frac{q^+}{100}\,(c_{max} - c_{min}) \right]$ and $\left[c_{max} - \frac{q^-}{100}\,(c_{max} - c_{min}); c_{max} \right]$), with a weighted linear least-square method with error in both coordinates [30]. h_- (resp. h_+) is the root of a 'pseudo second degree polynomial' ([30]), the coefficients of which depend themselves slightly on h_- ([30]):

$$A\,h_-^2 + B\,h_- + C = 0 \tag{55}$$

The solution $h_- = -21.6916 s^{\frac{1}{2}}.\mu m^{-1}$ is obtained, in our example, after 3 iterations from the non-weighted least-square slope $h_-^0 = -16.8775 s^{\frac{1}{2}}.\mu m^{-1}$ as initial value.

$$A = \sum_{i=1}^{N^-} \frac{w_i \left(\frac{x_i - x_M}{\sqrt{\Delta t}} - \frac{\langle x - x_M \rangle}{\sqrt{\Delta t}} \right) (U_i - \langle U \rangle)}{w \left(\frac{x_i - x_M}{\sqrt{\Delta t}} \right)} \tag{56}$$

$$B = \sum_{i=1}^{N^-} w_i^2 \left(\frac{\left(\frac{x_i - x_M}{\sqrt{\Delta t}} - \frac{\langle x - x_M \rangle}{\sqrt{\Delta t}} \right)^2}{w\,(U_i)} - \frac{(U_i - \langle U \rangle)^2}{w \left(\frac{x_i - x_M}{\sqrt{\Delta t}} \right)} \right) \tag{57}$$

$$C = -\sum_{i=1}^{N^-} \frac{w_i \left(\frac{x_i - x_M}{\sqrt{\Delta t}} - \frac{\langle x - x_M \rangle}{\sqrt{\Delta t}} \right) (U_i - \langle U \rangle)}{w\,(U_i)} \tag{58}$$

$$\tag{59}$$

where:
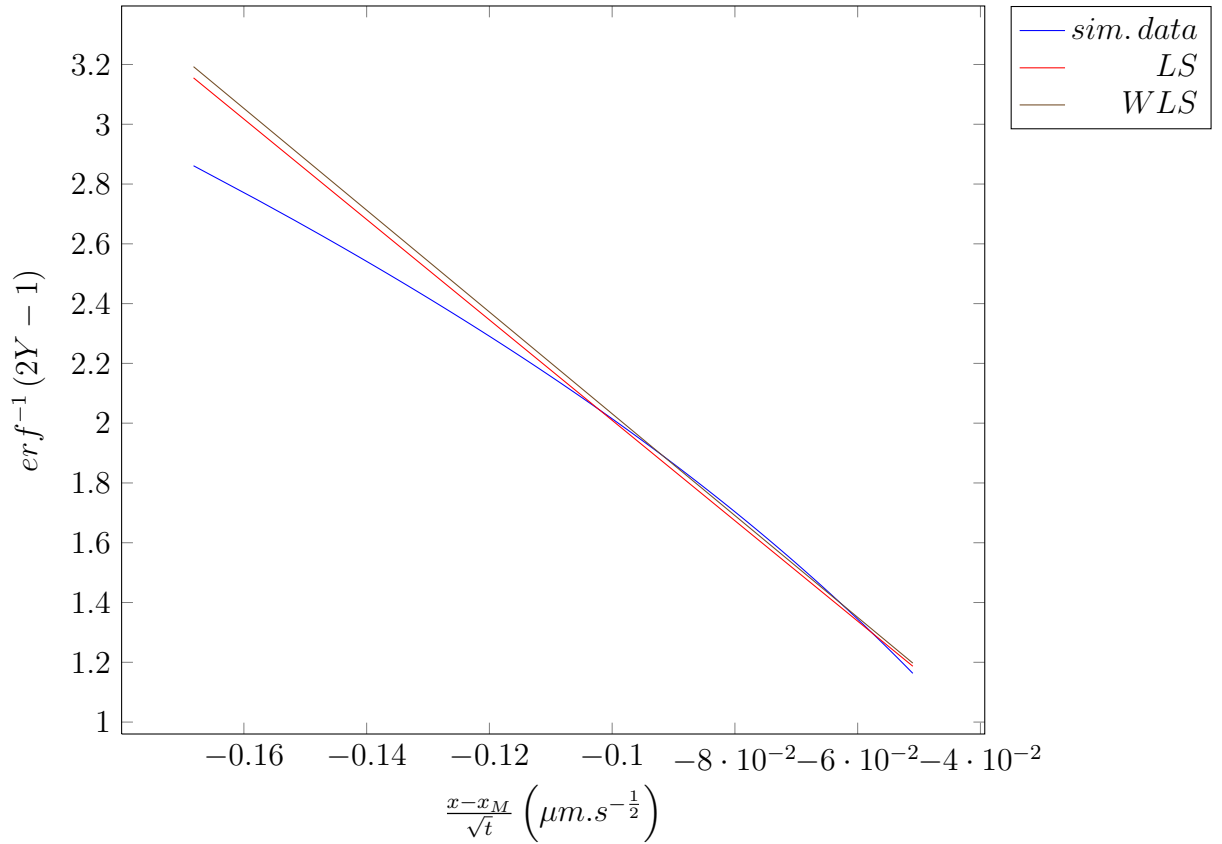- N^- is the number of points used to fit h_-,

Figure 10: Least square fitting of the example of the left hand side plateau (blue line) with non-weitghted (LS-red) and weighted (WLS-black) with error in both coordinates least-square methods

.

- global weight: $w_i = \dfrac{w\left(\frac{x_i - x_M}{\sqrt{\Delta t}}\right) w(U_i)}{h_-^2 w(U_i) + w\left(\frac{x_i - x_M}{\sqrt{\Delta t}}\right)}$,

- weight for x: $w\left(\dfrac{x_i - x_M}{\sqrt{\Delta t}}\right) \simeq \dfrac{1}{u(x_i)^2 + u(x_M)^2}$,

- weight for U: $w\left(U_i\right) = \dfrac{1}{\frac{dU}{dc}^2 u(c_i)^2}$

The uncertainty upon $\frac{(x_i - x_M)}{\sqrt{\Delta t}}$ is due to x_M, $u\left(x_M\right)$, and to the uncertainty upon x_i. This latter is obtained from that of $c\left(x_i\right)$: $u\left(x_i\right) = c^{-1}\left(c_i + u\left(c_i\right)\right) - \left(c_i - u\left(c_i\right)\right)$, whereas $u\left(U_i\right) = \frac{dU}{dc} u(c_i)$ with $\frac{dU}{dc} = \frac{\sqrt{\pi}}{c_{max} - c_{min}} e^{(2Y-1)^2}$.

Figure 10 shows as an example the weighted and non-weighted least-square fits of the left hand side plateau on our material. Weights are simply the

inverses of the uncertainties on both coordinates. The weighted method is believed to be closer to real values, which is hardly the case in our example but above all enables computating uncertainties upon h_+ and k_+ (*resp.* on h_- and k_-) which both depend on the abscissa uncertainty $u\left(\frac{x-x_M}{\sqrt{\Delta t}}\right)$ and on the ordinate uncertainty $u\left(U\right)$ deduced from $u(c)$. Once h_- is found k_- is obtained from:

$$k_- = \langle U \rangle - h_- \left\langle \frac{x_i - x_M}{\sqrt{\Delta t}} \right\rangle \tag{60}$$

Figure 11 gives Hall interdiffusion coefficient $\widetilde{D}$ as well as Boltzmann-Matano value. They are very close one to each other, probably partly because of the choice of the fitting function.

4.4. Uncertainty upon Hall interdiffusion coefficient

The uncertainty upon $\widetilde{D}$ is obtained by first expressing (53) and (54) as a function of concentration c instead of U.

$$\widetilde{D}_- = \frac{10^{-8}}{4\,h_-^2}\left[1 - 2\,k_-\,\sqrt{\pi}\,exp^{\left[erf^{-1}\left(\frac{2\,c-(c_{min}+c_{max})}{c_{max}-c_{min}}\right)\right]^2}\left(\frac{c_{max}-c}{c_{max}-c_{min}}\right)\right]\sin^2\alpha\,cm^2 s^{-1} \tag{61}$$

$$\widetilde{D}_+ = \frac{10^{-8}}{4\,h_+^2}\left[1 + 2\,k_+\,\sqrt{\pi}\,exp^{\left[erf^{-1}\left(\frac{2\,c-(c_{min}+c_{max})}{c_{max}-c_{min}}\right)\right]^2}\left(\frac{c-c_{min}}{c_{max}-c_{min}}\right)\right]\sin^2\alpha\,cm^2 s^{-1} \tag{62}$$

Hence, in the interval $\left[c_{max} - \frac{q^-}{100}\left(c_{max}-c_{min}\right) ; c_{max}\right]$, $u\left(\widetilde{D}\right)$ reads:

$$u\left(\widetilde{D}\right)^2 = \left(\frac{\partial\widetilde{D}}{\partial c}\right)^2 u\left(c\right)^2 + \left(\frac{\partial\widetilde{D}}{\partial\alpha}\right)^2 u\left(\alpha\right)^2 + \left(\frac{\partial\widetilde{D}}{\partial h_-}\right)^2 u\left(h_-\right)^2 + \left(\frac{\partial\widetilde{D}}{\partial k_-}\right)^2 u\left(k_-\right)^2 \tag{63}$$

with:

$$
\begin{aligned}
u(c)^2 &= \left(\tfrac{\partial c}{\partial\lambda_1}\right)^2 u\left(\lambda_1\right)^2 + \left(\tfrac{\partial c}{\partial\lambda_2}\right)^2 u\left(\lambda_2\right)^2 + \left(\tfrac{\partial c}{\partial x_0}\right)^2 u\left(x_0\right)^2 \\
&+ \left(\tfrac{\partial c}{\partial c(x_0)}\right)^2 u\left(c\left(x_0\right)\right)^2 + \left(\tfrac{\partial c}{\partial c'(x_0)}\right)^2 u\left(c'\left(x_0\right)\right)^2 + \left(\delta c\right)^2
\end{aligned} \tag{64}
$$

$u(k_-)$, $u\left(h_-\right)$, $u(k_+)$ and $u\left(h_+\right)$ are obtained by means of Reed least-square fitting method for pairs of coordinates ([30]). Since their expressions are rather cumbersome [30], they are not given here but they depend on the

same variables as h_- and k_-, i.e. A, B and C.

Tables 3 and 4 show that an approximate amount of 2000 points in the fitted area ($q_- = q_+ = 20$ for the width of the fitting intervals) is sufficient to determine h_-, k_-, h_+, k_+ and their uncertainties.

N	$h_- \left(s^{\frac{1}{2}}.\mu m^{-1}\right)$	$u\left(h_-\right) \left(s^{\frac{1}{2}}.\mu m^{-1}\right)$	k_-	$u\left(k_-\right)$
300	-16.5665	0.0737749	0.361792	0.00569403
2000	-16.9767	0.0189383	0.332352	0.00146226
4000	-17.0093	0.0126968	0.330016	0.000980421
10000	-17.0272	0.00777959	0.328728	0.000600755

Table 3: Sensitivity of h_-, k_- and their uncertainties to the number of points N_-

N	$h_+ \left(s^{\frac{1}{2}}.\mu m^{-1}\right)$	$u\left(h_+\right) \left(s^{\frac{1}{2}}.\mu m^{-1}\right)$	k_+	$u\left(k_+\right)$
300	-12.1487	0.0456292	-0.481375	0.0040949
2000	-12.3394	0.012405	-0.465739	0.00111574
4000	-12.3543	0.0084178	-0.464517	0.000757272
10000	-12.3625	0.0051977	-0.463844	0.00046764

Table 4: Sensitivity of h_+, k_+ and their uncertainties to the number of points N_+

The sensitivity of $\widetilde{D}$ uncertainty to its different causes are given by the partial derivatives:

- $\frac{\partial \widetilde{D}}{\partial c} \frac{\partial c}{\partial \lambda_1}$ for changes in λ_1,

...

- $\frac{\partial \widetilde{D}}{\partial c} \frac{\partial c}{\partial c'(x_0)}$ for changes in $c'(x_0)$,

- $\frac{\partial \widetilde{D}}{\partial c}$ for changes in c due to EPMA averaging effect,

- $\frac{\partial \widetilde{D}}{\partial \alpha}$ for changes in α, due to α assessment uncertainty

- $\frac{\partial \widetilde{D}}{\partial h_-}$ for changes in h_-, the uncertainty of which is given by the weighted least-square method with error in both coordinates,

- $\frac{\partial \widetilde{D}}{\partial k_-}$ for changes in k_-.

From (53) it is noticeable that $\frac{\partial \widetilde{D}}{\partial c}$ can be obtained in the following way:

$$\frac{\partial \widetilde{D}_-}{\partial c} = \left(\widetilde{D}_- + \frac{k_- - 1}{2\,h_-^2}\right) \frac{dU}{dc} = \left(\widetilde{D}_- + \frac{k_- - 1}{2\,h_-^2}\right) \frac{\sqrt{\pi}}{c_{max} - c_{min}} e^{(2\,Y - 1)^2} \quad (65)$$
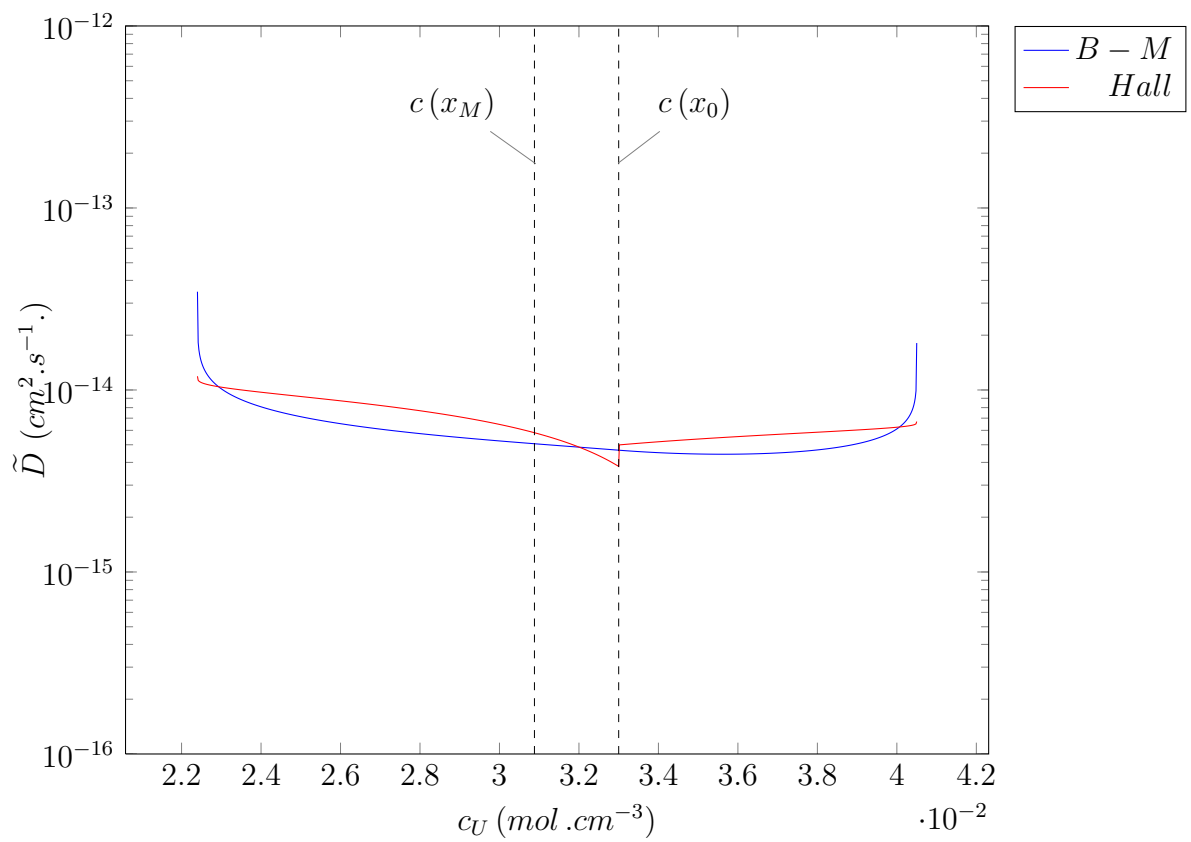
Figure 11: Comparison of Hall and Boltzmann-Matano interdiffusion coefficient ($\widetilde{D}$) as a function of uranium concentration (c_U)
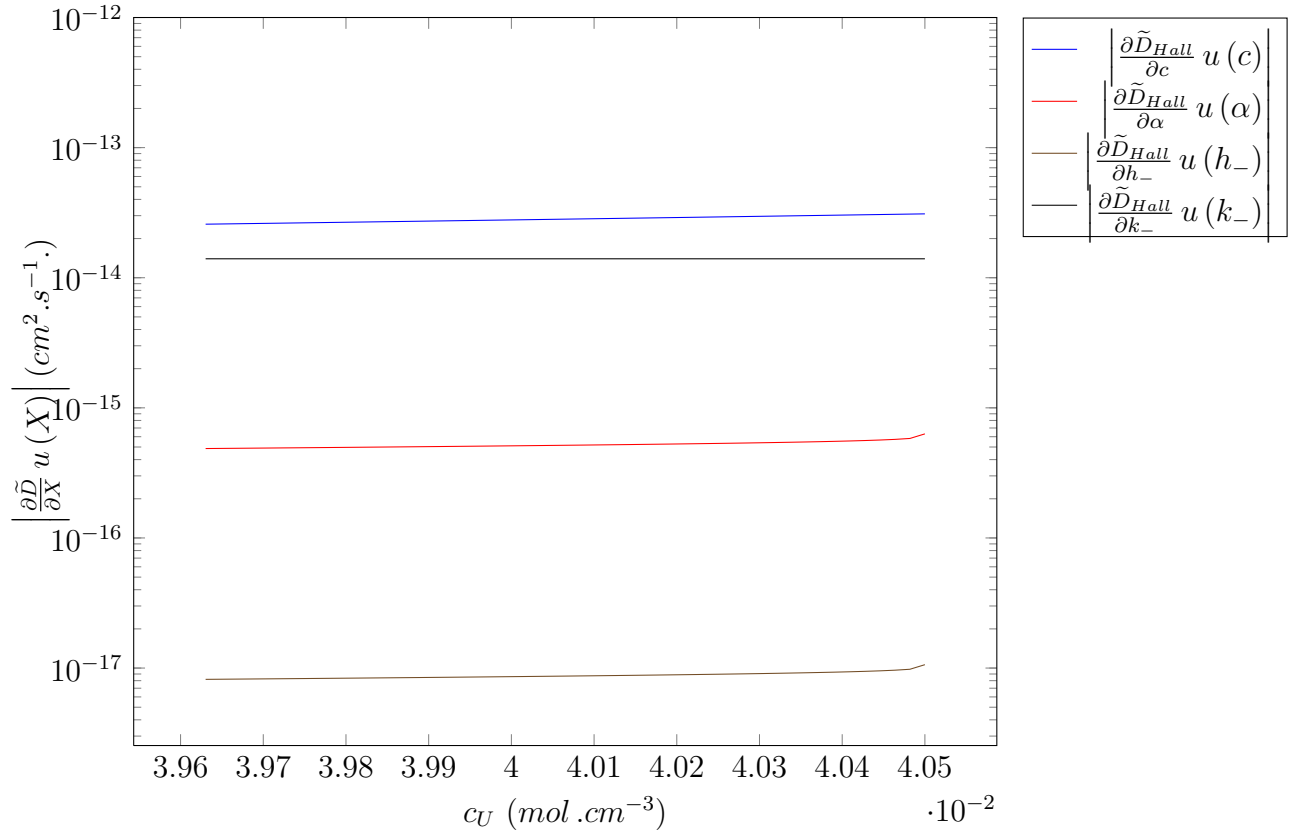
.

Figure 12: Contribution of c, α, h_- and k_- to Hall $\widetilde{D}_-$ coefficient

The analog result also stands for $\frac{\partial \widetilde{D}_+}{\partial c}$.

$\frac{\partial c}{\partial \lambda_1}, ..., \frac{\partial c}{\partial'_{\cdot(x_0)}}$ are obtained like in the case of Boltzmann-Matano method. For the last three partial derivatives analytical expressions can be used:

$$\frac{\partial \widetilde{D}}{\partial \alpha} = 2\, cotg\,(\alpha)\, \widetilde{D} \tag{66}$$

$$\frac{\partial \widetilde{D}}{\partial h} = -\frac{2\,\widetilde{D}}{h} \tag{67}$$

$$\frac{\partial \widetilde{D}}{\partial k} = \frac{\widetilde{D}}{k} - \frac{1}{4k\,h^2} \tag{68}$$

A noticeable property of these first two partial derivatives is that they vary

in the same way as $\widetilde{D}$ does, so that their corresponding contribution to $u\left(\widetilde{D}\right)$ is minimum as $\widetilde{D}$ reaches its minimum. It does not apply for the last one since $\forall c,\ \widetilde{D}_-(c) \leqslant \frac{1}{4h_-^2}$ and $\lim_{x\to-\infty} \widetilde{D}_- = \frac{1}{4\,h_-^2}$ (resp. $\widetilde{D}_+(c) \leqslant \frac{1}{4h_+^2}$ and $\lim_{x\to+\infty} \widetilde{D}_+ = \frac{1}{4\,h_+^2}$). Figure 12 gives the relative contribution of each cause to Hall estimation of the Hall interdiffusion coefficient versus concentration for the left hand side of the profile.

The main causes of error are the uncertainty upon k_- (resp. k_+) and upon c (due to those of the fitting parameters, this latter is overestimated, since uncertainties on the concentration function 18 parameters cannot all take a bad value at the same time otherwise the curve fitting would not be acceptable).

Although $\widetilde{D}(c)$ obtained by Hall method has got rather high incertitude values (close do $10^{-14} cm^2 s^{-1}$ in our example) as c varies, its limits which do not depend on c are more precise. The assessed limits of $\widetilde{D}$ obtained on our profile are the following:

$$\lim_{x\to-\infty} \widetilde{D}_- = 8.75 \pm 0.806 \cdot 10^{-15}\, cm^2 s^{-1} \tag{69}$$

$$\lim_{x\to+\infty} \widetilde{D}_+ = 1.66 \pm 0.052 \cdot 10^{-14}\, cm^2 s^{-1} \tag{70}$$

5. Discussion

The three coefficients are very close and in good agreement in the range of $[0.0226; 0.0403]\, mol\,.cm^{-3}$. Below and over these values Hall diffusion coefficient has to be preferred.

The function 18 used in this work in order to fit interdiffusion profiles is very sensitive to the values chosen at the inflexion point (x_0, $c\left(x_0\right)$ and $c'\left(x_0\right)$). Its asymptots depend both on well known compositions at each end and on the values of the parameters sensitive to function variations at the inflexion points. Thus the parameters adjusted for the fitting function were precise enough to fit the asymptots so that den Broeder (or even Boltzmann-Matano) method could be very close to Hall method. The use of an analytical function for the three cases permitted the use of as many points as needed in function of the part of the curve (equally spaced as a function of x position or of concentration c value).

6. Conclusion

A way of computing uncertainty associated to Boltzmann-Matano, den Broeder and Hall methods has been proposed for assessing volume inter-diffusion coefficients changes with composition from Electron Probe Micro-analyser measurements on polycrystalline materials. This method has been used by S. Noyau [20] in order to study $UO_2/U_{1-y}Pu_yO_{2-z}$ interdiffusion in the temperature range 1500°C-1700°C. In the particular case of our material $U_{1-y}Pu_yO_{2-z}$ and experimental conditions (1700°C), the three methods have given agreeing results and the uncertainty study has given a concentration range for which the EPMA profile results could be reliably used.

In the central part of the concentration range, both den Broeder and Boltzmann-Matano methods give the same results with an uncertainty close to $8 \cdot 10^{-15} cm^2 \cdot s^{-1}$ while they both fail at the ends of this concentration range where Hall method give better results with an uncertainty close to $8 \cdot 10^{-16} cm^2 \cdot s^{-1}$. For these very small volume interdiffusion coefficients the choice of an aquisition line making a very small angle with the interdiffusion interface has lead to an enhanced precision on the fitted parameters of the concentration smoothing function. An optimized angle has to be chosen since interdiffusion profiles with a small angle with the interface otherwise decrease the precision upon interdiffusion coefficients.

In the central part of the interdiffusion profiles in our case of study values smaller than $10^{-14} cm^2 \cdot s^{-1}$ can hardly be measured. This value is also close to the lower limit of what can be obtained in terms of Hall interdiffusion coefficient on the plateaus of the interdiffusion profiles.

Single crystals could be used as benchmark materials in order to check the validity of the results as well as their precision.

A way of enhancing precision in the interdiffusion coefficient values versus concentration would be to use several interdiffusion couples with intermediate compositions.

The C/C++-language software developed in this work is available on request for whom is interested in.

7. Acknoledgements

[1] L. Boltzmann ,L., Zur Integration der Diffusiongleichung bei variabeln Diffusioncoefficienten, Wiedemann's Ann. Phys. 53 (1894) 959–964.

[2] Matano, Chujiro, On the Relation between the Diffusion-Coefficients and Concentrations of Solid Metals (The Nickel-Copper System), Japanese Journal of Physics 8 (1933) 109.

[3] F. den Broeder, A general simplification and improvement of the matano-boltzmann method in the determination of the interdiffusion coefficients in binary systems, Scripta Metallurgica 3 (5) (1969) 321–325, ISSN 0036-9748, doi:10.1016/0036-9748(69)90296-8.

[4] L. D. Hall, An Analytical Method of Calculating Variable Diffusion Coefficients, The Journal of Chemical Physics 21 (1) (1953) 87–89, ISSN 00219606, doi:doi:10.1063/1.1698631.

[5] J.-F. Cornet, Résolution numérique de l'équation de Fick lorsque le coefficient de diffusion chimique dépent de la concentration. Détermination des coefficients de diffusion chimique à partir de la courbe concentration-pénétration et restitution de cette courbe à partir des premiers, en milieux infinis, Premier Ministre, Commissariat l'énergie atomique ; Rapport CEA R-4369. Division de métallurgie et d'étude des combustibles nucléaires. Centre d'études Nucléaires de Fontenay-aux-Roses, Centre d'études nucléaires, Service de documentation, Saclay, 1972.

[6] D. Glasserleme, H. Matzke, Dependence upon oxygen potential of the interdiffusion in single crystalline UO2-(U, Pu)O2, Solid State Ionics 12 (1984) 217–225, ISSN 01672738, doi:10.1016/0167-2738(84)90150-4, URL http://65.54.113.26/Publication/18575030/dependence-upon-oxygen-potential-of-t

[7] T. M. Besmann, T. B. Lindemer, Chemical thermodynamic representations of $\langle PuO_{2-x} \rangle$ and $\langle U_{1-z}Pu_zO_w \rangle$, Journal of Nuclear Materials 130 (0) (1985) 489 – 504, ISSN 0022-3115, doi:10.1016/0022-3115(85)90335-6, URL http://www.sciencedirect.com/science/article/pii/0022311585903356.

[8] T. Besmann, T. Lindemer, Improvement in the chemical thermodynamic representation of $\langle PuO_{2-x} \rangle$ and $\langle U_{1-z}Pu_zO_w \rangle$, Journal of Nuclear Materials 137 (3) (1986) 292 – 293,

ISSN 0022-3115, doi:10.1016/0022-3115(86)90232-1, URL `http://www.sciencedirect.com/science/article/pii/0022311586902321`.

[9] C. Guéneau, N. Dupin, B. Sundman, C. Martial, J.-C. Dumas, S. Gossé, S. Chatain, F. D. Bruycker, D. Manara, R. J. Konings, Thermodynamic modelling of advanced oxide and carbide nuclear fuels: Description of the UPuOC systems, Journal of Nuclear Materials 419 (13) (2011) 145 – 167, ISSN 0022-3115, doi:10.1016/j.jnucmat.2011.07.033, URL `http://www.sciencedirect.com/science/article/pii/S0022311511007446`.

[10] J. H. Harding, D. G. Martin, P. E. Potter, R. Commission of the European Communities. Directorate-General for Science, Thermophysical and thermochemical properties of fast reactor materials, Commission of the European Communities, Directorate-General Science, Research and Development, Luxembourg, ISBN 9282608298 9789282608296, 1989.

[11] S. Kailasam, J. Lacombe, M. Glicksman, Evaluation of the methods for calculating the concentration-dependent diffusivity in binary systems, Metallurgical and Materials Transactions A 30 (10) (1999) 2605–2610, ISSN 1073-5623, doi:10.1007/s11661-999-0300-9.

[12] B. Messerschmidt, B. McIntyre, S. Houde-Walter, R. R. Andre, C. Hsieb, Temperature dependence of silver-sodium interdiffusion in micro-optic glasses, Optical Materials 7 (4) (1997) 165–171, ISSN 0925-3467, doi:10.1016/S0925-3467(97)00018-9, URL `http://www.sciencedirect.com/science/article/pii/S0925346797000189`.

[13] Sandrine Mendez, Etude de l'inerdiffusion U-Pu appliquée au combustible MOX, Ph.D. thesis, Aix-Marseille 3, 1995.

[14] A. G. Nikitin, S. V. Spichak, Y. S. Vedula, A. G. Naumovets, Symmetries and modelling functions for diffusion processes, Journal of physics. D, Applied physics 42 (5), ISSN 0022-3727.

[15] R. Hooke, T. A. Jeeves, Direct Search Solution of Numerical and Statistical Problems, J. ACM 8 (2) (1961) 212229, ISSN 0004-5411, doi:10.1145/321062.321069, URL `http://doi.acm.org/10.1145/321062.321069`.

[16] R. B. Marinenko, S. D. Leigh, Uncertainties in Electron Probe Microanalysis, in: European Microbeam Analysis Society 2009, vol. 7, Gdansk, 1–10, 2010.

[17] F. Sauer, Z. Freise, Diffusion in Binary Mixtures Showing a Volume Change, Z. Elektrochem. 66 (1962) 353–363.

[18] C. Wagner, The evaluation of data obtained with diffusion couples of binary single-phase and multiphase systems, Acta Metallurgica 17 (2) (1969) 99–107, ISSN 0001-6160, doi:10.1016/0001-6160(69)90131-X.

[19] H. Matzke, Rutherford backscattering for measuring corrosion layers on glasses for long-term storage of radioactive waste, Fresenius' Journal of Analytical Chemistry 319 (6) (1984) 801–808, ISSN 0937-0633, doi:10.1007/BF01226776, URL http://www.springerlink.com/content/n7w884w6pq551470/abstract/.

[20] S. Noyau, Etude des phénomènes d'autodiffusion et d'interdiffusion du plutonium dans des céramiques de type $U_{1-y}Pu_yO_{2\pm x}$, Thèse de doctorat, Université de Limoges, Limoges, URL http://www.sudoc.fr/xxxxxxxx, 2012.

[21] Y. Zhang, M. J. Kramer, D. Banerjee, I. Takeuchi, J. Ping Liu, Transmission electron microscopy study on Co/Fe interdiffusion in SmCo5/Fe and Sm2Co7/Fe/Sm2Co7 thin films, Journal of Applied Physics 110 (5) (2011) 053914–053914–4, ISSN 00218979, doi:doi:10.1063/1.3634063.

[22] F. Guillemot, J. Debuigne, Etude Metallurgique d'Alliages de Titane pour Applications Biomedicales, These de doctorat, Universite de Rennes, Rennes, URL http://www.sudoc.fr/071052046, 2000.

[23] I. Thibon, D. Ansel, T. Gloriant, Interdiffusion in -TiZr binary alloys, Journal of Alloys and Compounds 470 (12) (2009) 127–133, ISSN 0925-8388, doi:10.1016/j.jallcom.2008.02.082, URL http://www.sciencedirect.com/science/article/pii/S0925838808003095.

[24] Palcut, Marián, Cation diffusion in LaMnO3 , LaCoO3 and LaFeO3 materials, Ph.D. thesis, Norwegian University of Science and Technology, Trondheim, URL http://ntnu.diva-portal.org/smash/get/diva2:123258/FULLTEXT01, 2007.

[25] M. Dupuy, Diffusion dans le système uranium-plutonium et autodiffusion du plutonium epsilon, impr. L. Jean, Gap, URL `http://www.sudoc.fr/08900082X`, 1968.

[26] A. Laik, G. Kale, K. Bhanumurthy, Interdiffusion studies between a Mo-based alloy and Ti, Metallurgical and Materials Transactions A 37 (10) (2006) 2919–2926, ISSN 1073-5623, doi:10.1007/s11661-006-0173-0, URL `http://www.springerlink.com/content/wn23367250680j27/abstract/`.

[27] R. Rettig, S. Steuer, R. Singer, Diffusion of Germanium in Binary and Multicomponent Nickel Alloys, Journal of Phase Equilibria and Diffusion 32 (3) (2011) 198–205, ISSN 1547-7037, doi:10.1007/s11669-011-9853-6, URL `http://www.springerlink.com/content/f65t1k8753512u01/abstract/`.

[28] L. Feng, L. Huand, H. Chang, Y. Cui, L. Zhou, Interdiffusion behavior of Ti-Mo binary system in β phase, The Chinese Journal of Nonferrous Metals ISSN 1004-0609, doi:CNKI:SUN:ZYXZ.0.2009-10-011.

[29] R. Anand, C. Sudha, S. Saroja, A. L. E. Terrance, M. Vijayalakshmi, Simulation of carbon diffusion profile in dissimilar weldment of ferritic steels using diffusion coefficients evaluated by den Broeders method, in: METAL2008, Hradec nad Moravic, ISBN 978-80-254-1987-8, 1–10, URL `http://www.metal2011.com/data/metal2008/sbornik/Lists/Papers/173.pdf`, 2008.

[30] B. C. Reed, Erratum: Linear least-squares fits with errors in both coordinates [Am. J. Phys. 57, 642646 (1989)], American Journal of Physics 58 (2) (1990) 189, ISSN 00029505, doi:10.1119/1.16506.